T.C.
FATIH UNIVERSITY
INSTITUTE OF BIOMEDICAL ENGINEERING

DETECTION OF THE OPTIC DISC FROM THE DIABETIC MACULAR EDEMA PATIENTS' RETINAL IMAGES

RAZİYE YAĞIZ

MSc THESIS
BIOMEDICAL ENGINEERING PROGRAMME

ISTANBUL, JUNE / 2013

T.C.
FATIH UNIVERSITY
INSTITUTE OF BIOMEDICAL ENGINEERING

DETECTION OF THE OPTIC DISC FROM THE DIABETIC MACULAR EDEMA PATIENTS' RETINAL IMAGES

RAZİYE YAĞIZ

MSc THESIS
BIOMEDICAL ENGINEERING PROGRAMME

THESIS ADVISOR
ASSIST. PROF. DR. ŞÜKRÜ OKKESİM

ISTANBUL, JUNE / 2013

T.C.
FATİH ÜNİVESİTESİ
BİYOMEDİKAL MÜHENDİSLİK ENSTİTÜSÜ

DİYABETİK MAKULAR ÖDEMLİ HASTALARIN RETİNAL
GÖRÜNTÜLERİNDEN OPTİK DİSKİN BELİRLENMESİ

RAZİYE YAĞIZ

YÜKSEK LİSANS TEZİ
BİYOMEDİKAL MÜHENDİSLİĞİ PROGRAMI

DANIŞMAN
YRD. DOÇ. DR. ŞÜKRÜ OKKESİM

İSTANBUL, HAZİRAN / 2013

T.C.

FATIH UNIVERSITY

INSTITUTE OF BIOMEDICAL ENGINEERING

Raziye Yağız, a **MSc** student of Fatih University **Institute of Biomedical Engineering** student ID **52011101**, successfully defended the **thesis** entitled "**DETECTION OF THE OPTIC DISC FROM THE DIABETIC MACULAR EDEMA PATIENTS' RETINAL IMAGES**'', which she prepared after fulfilling the requirements specified in the associated legislations, before the jury whose signatures are below.

Thesis Advisor :   **Assist. Prof. Dr. Şükrü OKKESİM**

Fatih University

Jury Members: **Prof. Dr. Sadık KARA**   ....

Fatih University

Assist. Prof. Dr. Kadir TUFAN

Fatih University

Date of Submission :   **17 May 2013**
Date of Defense :   **11 June 2013**

ACKNOWLEDGEMENTS

First of all, I wish to express my sincere gratitude and reverence to Assist. Prof. Dr. Şükrü Okkesim, my supervisor who guided this work and helped me whenever I was in need. His direction and support have been invaluable, not only in work but also in life experience. I thank him for his guidance, encouragement, tolerance and freedom of work.

I wish to express my sincere thanks to Mustafa Selman Yıldırım and Emine Doğanay for their guidance advice, encouragement and support throughout my thesis.

Last but not least, I am highly indebted to my parents for giving me the strength of will to pursue what I believed and for giving me strength of character to lead a righteous life. Without them and all the sacrifices they made, I wouldn't be the same person.

June 2013   Raziye YAĞIZ

TABLE OF CONTENTS

1. INTRODUCTION

2. SECOND CHAPTER

LITERATURE REVİEW

3.THIRD CHAPTER

MATERİALS AND METHODS

4. FOURTH CHAPTER

APPENDICES

LIST OF SYMBOLS

$\times$	Cross sign
μ	Mean
$+$	Plus sign
σ	Standard Deviation
Δ	Triangular shape

ABBREVIATIONS

DME   : Diabetic Macular Edema
DM   : Diabetes Mellitus
DR   : Diabetic Retinopathy
ELVD   : Elliptical Local Vasculature Density
ETDRS   : Early Treatment Diabetic Retinopathy Study Research Group
HEI-MED   : Hamilton Eye Institute Macular Edema Dataset
NPDR   : Non-Proliferative Diabetic Retinopathy
OD   : Optic disc
PDR   : Proliferative Diabetic Retinopathy
SE   : Structuring element

LIST OF FIGURES

LIST OF TABLES

SUMMARY

DETECTION OF THE OPTIC DISC FROM THE DIABETIC MACULAR EDEMA PATIENTS' RETINAL IMAGES

Raziye YAĞIZ

Biomedical Engineering Programme

MSc. Thesis

Advisor: Assist. Prof. Şükrü OKKESİM

Diabetic retinopathy (DR) is a vascular complication in the eyes of diabetic mellitus. Diabetic macular edema (DME) is the most common cause of vision loss among the complications of DR. Optic disc (OD) detection is a crucial step in automated screening systems for diabetic macular edema. Because of the similar image properties between OD and exudate, OD center cannot be determined properly.

In this thesis, three different methods based on Hough and mathematical morphology are presented to automatically detect the center of the OD from the diabetic macular edema patients' fundus images. All methods have been tested on 169 hard exudates and non hard exudates images which taken from a publicly-available database and obtained results are compared.

Our experimental results indicate that method III can exactly determine the center of the OD from 139 fundus images especially for color hard exudates images. On the other part, all three methods cannot detect the OD center for the rest of 30 images.

Keywords: Diabetic Macular Edema, Optic Disc Detection, Image Processing.

FATIH UNIVERSITY - INSTITUTE OF BIOMEDICAL ENGINEERING

ÖZET

DİYABETİK MAKULAR ÖDEMLİ HASTALARIN RETİNAL GÖRÜNTÜLERİNDEN OPTİK DİSKİN BELİRLENMESİ

Raziye YAĞIZ

Biyomedikal Mühendisliği Programı
Yüksek Lisans Tezi

Danışman: Yrd. Doç. Şükrü OKKESİM

Diyabetik retinopati (DR) diyabet hastalığında gözde oluşan damarsal bir komplikasyondur. Diyabetik makular ödem (DME) DR komplikasyonları arasında görme kaybının en sık nedenidir. Optik diskin (OD) belirlenmesi, diyabetik makular ödem tanısı için kullanılan otomatik görüntüleme sistemlerinde önemli bir adımdır. OD ve eksuda arasındaki benzer görüntü özelliklerinden dolayı , OD merkezi doğru bir şekilde tespit edilememektedir.

Bu tezde, Hough ve matematiksel morfolojiye dayanan üç farklı yöntem diyabetik makular ödemli hastaların fundus görüntülerinden OD merkezinin belirlenmesi için incelenmiştir. Bütün metodlar halka açık olan bir veritabanından alınan 169 sert eksudalı ve sert eksudalı olmayan görüntüler üzerinde test edilmiş ve elde edilen sonuçlar karşılaştırılmıştır.

Hesaplanan veriler metod III'ün 139 fundus görüntüsü üzerinde özellikle sert eksudalı görüntülerde OD merkezini belirlemede daha iyi sonuçlar verdiğini göstermektedir. Diğer taraftan kalan 30 fundus görüntüsü için her üç metot da OD merkezini belirleyememektedir.

Anahtar kelimeler: Diyabetik Makular Ödem, Optik Disk Belirleme, Görüntü İşleme.

FATİH ÜNİVERSİTESİ -BİYOMEDİKAL MÜHENDİSLİK ENSTİTÜSÜ

CHAPTER 1

INTRODUCTION

1.1. Purpose of the thesis

Diabetes Mellitus (DM) is a chronic disorder and it can be characterized by the impaired metabolism of glucose because of insulin shortage or its resistance. DM leading to hyperglycemia and therefore there are many complications that can affect the eyes and nervous system, as well as the heart, kidneys and other organs in DM patient [1].

There are two types DM called type 1 and type 2. Type 1 is primarily caused by autoimmune pancreatic b-cell devastation and characterized by absolute insulin shortage, and type 2 characterized by insulin resistance and relative insulin shortage [1].

Diabetic retinopathy (DR) is a vascular complication in the eyes of DM. It damages the retina, thus causes the vision loss. For any type of diabetes, the occurrence of diabetic retinopathy in people more than 40 years of age was reported to be 40.3% [2].

Diabetic macular edema (DME) is the most common cause of vision loss among the complications of DR [3]. DME is defined as swelling of the retina. To prevent vision loss doctors want to diagnose the DME as early as, but there are a lot of diabetic patients and the number of diabetic patients is growing day by day. In addition, costs of the current detection methods are too much to achieve the screening compliance in at-risk populations. Instead, an automated system which uses image processing techniques and artificial intelligence method to diagnose DR and DME is a potential key to this difficulty [3].

Therefore, there are a lot of studies for the early diagnosis of DME and several algorithms are suggested in literature [4-6].

Optic Disc is the entrance of the vessels, where the optic nerve exists in the eye, and it is usually a bright oval shaped object [7].

It appears in color fundus images as a bright yellowish or white region. Its size varies from patient to patient and its shape is more or less circular, and sometimes the optic disc has the form of an ellipse [8]. Detection of OD is an essential step for the early diagnosis of DME, because the OD location may help to determine the clinical relevance of lesions. If the OD location is unknown, parts of the OD can potentially be detected as a lesion and such false responses can be avoided.

In the literature, a large number of methods have been proposed for the detection of the OD. In this thesis, first of all we focused on the detection of the OD and then we evaluate the two methods which proposed in the literature and finally a new method was proposed and compared with other two methods.

1.2. Arrangement of the Thesis

This thesis is set up as follows:

_In the next chapter, information about the human retina, the appearance of the retinal, image and image processing is presented.

_In the third chapter, two automatic OD-detection methods are implemented as described in literature and newly developed method is presented. And also dataset is described.

_In the fourth chapter, obtained results using the implemented methods are discussed.

CHAPTER 2

LITERATURE REVİEW

This section will discuss about the structure of the eye, definition of diabetic retinopathy (DR) and its diagnosis and treatment methods, and then definition of macular edema, and finally definition of image and image processing.

2.1 Anatomy of the Eye

The eye is an organ that gives the sense of sight. Using the reflecting light, brain is able to interpret the shapes, colors, and dimensions of items. Instead, the fundamental organ which can see is brain and eye can only detect the light or dim light so it cannot sense an object when light is absent [10]. The eye is a hollow, spherical structure with a diameter of 2.5 cm and its weight about 7 grams. This structure has a wall consisting of three layers. The inner spaces of the eye are filled with fluids that support the walls and protect the structure of the eye [9]. In Figure 2.1, a cross-section of the human eye is shown with the anatomy labeled [10].

The eyes are so crucial due to the brain receives the four-fifth of all of the information, coming from the eyes. Information comes to the brain through the following steps. Light that passes through the iris is focused onto the retina through a lens. During this process, the visual information is encoded and transmitted to the brain through the optical nerve [11].

There are several structures which compose the human eye, however for the work presented in this thesis the retina is the most important part of the eye. The retina is a thin layer of neural cells that lines the back of the eye. It is light sensitive and absorbs light. It has duties of the transmit and receive image signals from the brain. The retina consists of two types of light receptors which called rods and cones. The rods absorb

light in black and white, whereas the cones are color sensitive and absorb stronger light. While the rods provide night vision, the cones are involved in color vision.

The optic disc (OD), also known as the optic nerve head or the blind spot, is a region where the optic nerve connects to the eye [12]. There are no light sensitive rods or cones which correspond to a light stimulus at this point. Therefore, it occurs a break in the field of the vision called "the blind spot" or the "physiological blind spot" [13]. The location of the optic disc is shown in Figure 2.2.
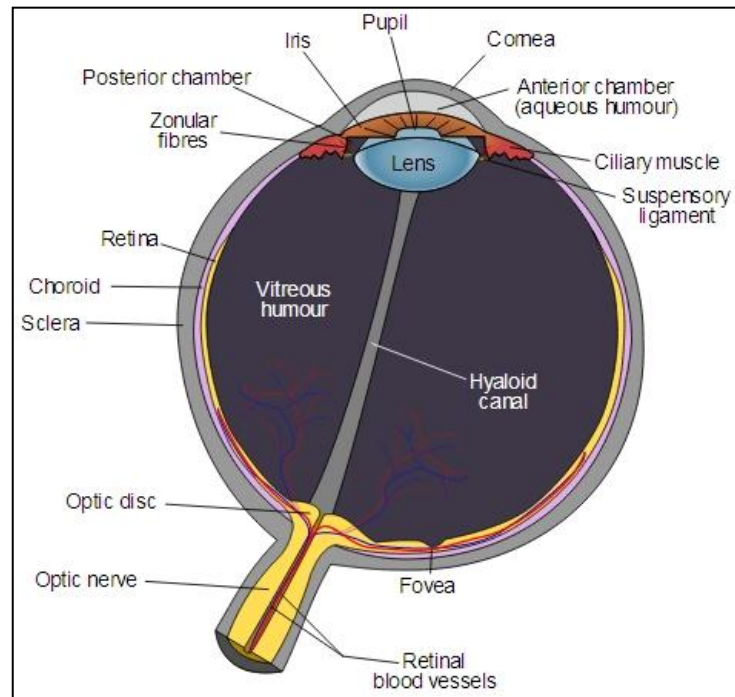
Figure 2.1 Anatomy structure of the eye [14].

The macula is the dark area in the vicinity of the fovea [12]. It is where located next to the center of the retina, an oval-shaped highly pigmented yellow spot [15] as shown in Figure 2.2. It is a small and highly sensitive part of the retina, which is responsible for detailed central vision.

The fovea is in the center of the macula. It is a small pit which contains packed tightest the visual cells. Therefore the fovea is responsible for optimal sharpness of vision. In contrast the retina, fovea contains blood vessels which are not involved in the passage of light striking [16]. Figure 2.2 shows the location of fovea.
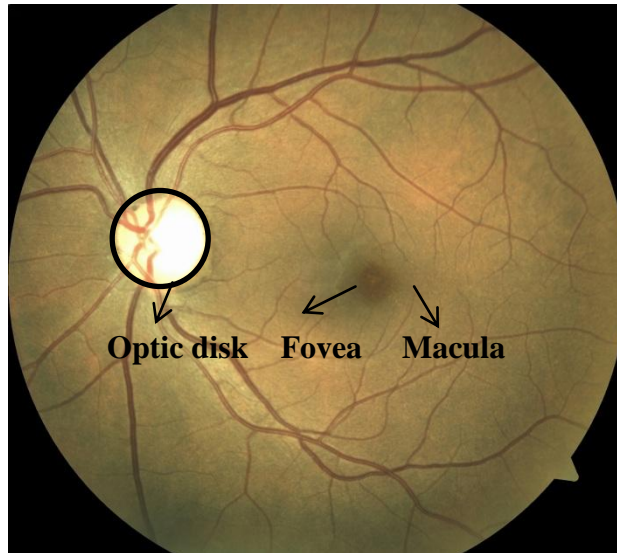
Figure 2.2   Location of macula, fovea and optic disc

2.2   Diabetic Retinopathy

Diabetes is the chronic condition caused by abnormal increase in the blood glucose level and which damages to the blood vessels in the body. The capillaries that nourish the retina, is damage due to increased glucose levels [17]. Diabetic retinopathy (DR) is one of the most important complications affecting the retinal capillaries. This effect causes to occur thickening of arterial wall and obstruction of blood flow in the eye.

DR generally can be divided into two classes; non-proliferative diabetic retinopathy (NPDR) and proliferative diabetic retinopathy (PDR) [17]. Stages of DR are summarized in Figure 2.3. NPDR is characterized by microaneurysm, exudate, hemorrhages and microinfarcts. This further can be classified into mild, moderate and severe depending on the extent of these changes. PDR is the advanced stage of diabetic retinopathy. It is characterized by new vessel formation commonly arising on the optic disk (new vessels on the disk) or arises on other parts of the retina (new vessel elsewhere) induced by ischemic changes in the retina and an imbalance between angiogenic and antiangiogenic factors [1].

DR consists of four stages:

Stage 1 – Background diabetic retinopathy (also termed mild or moderate non-proliferative retinopathy). There is at least one microaneurysm with or without the existence of retinal hemorrhages, hard exudates, cotton wool spots or venous loops [18, 19].

Stage 2 – Moderate non-proliferative retinopathy. There are numerous microaneurysms and retinal hemorrhages. Cotton wool spots and a certain amount of venous beading can also be occurred [17]. Some of the blood vessels are starting to become blocked.

Stage 3 – Severe non-proliferative retinopathy. Many features such as hemorrhages and microaneurysms are present in the retina. Other features are also present except less growth of new blood vessels; many more blood vessels are now blocked and these areas of the retina start to send signals to the body to grow new blood vessels for nourishment [20].

Stage 4 – Proliferative retinopathy. PDR is the advanced stage where the fluids sent by the retina for nourishment trigger the growth of new blood vessels [21]. The main blood vessels become stiff and blockage of blood flow occurs. Small pockets of blood begin to form around the boundary of the main blood vessels. These fragile blood vessels have thin walls and when the walls burst, blood leak out. Exudates (proteins and other lipids) and blood from the leakage forms around the retina and in some cases, leakage may form on the fovea, are some of the reason sudden severe vision loss and blindness.
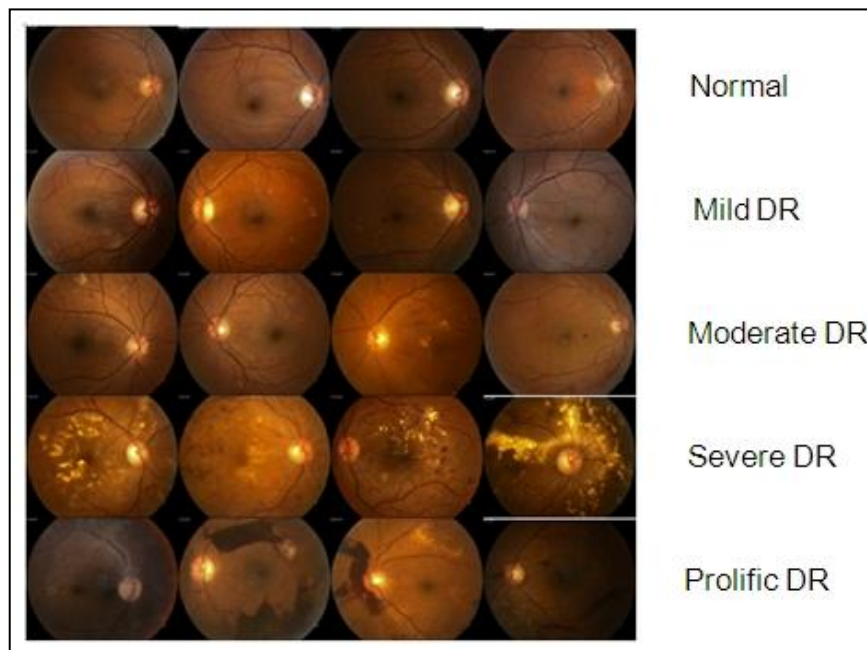
Figure 2.3 Stages of DR in fundus images [22].

There are many features which occur in a DR eye. However, since the main objective of this project is not to have an automated system for early DR detection on some of the extracted features. Therefore, features such as microaneurysms, exudates, hemorrhages, cotton wool spots and drusen will be discussed briefly.

Microaneurysms are small saclike out pouching in the small vessels and capillaries [23]. They are an early feature of DR. It appears as small red dots in fundus photograph because of the swelling of capillaries [24]. These features can leak fluid and blood into the retina and therefore it causes of vision threatening exudates, macular edema and hemorrhages.

Hard exudates or Intra-retinal lipid exudates are yellow deposits of lipoproteins within the sensory retina [25] as shown in figure 2.4. They appear as yellow-white dots within the retina. The yellow deposits may be seen as either individual spots or clusters [23] and they usually place near the OD.

Sometimes the exudates may be formed on macula or fovea, as a result, there will be sudden loss of vision in that eye, regardless of the diabetic retinopathy stages. They leak into retinal tissue with serum, and when serum is absorbed exudates are left behind as edema [24].

Exudates are the landmarks for the diagnosis of macular edema from single fundus image because they indicate increased vessel permeability and presence of fluid [25].
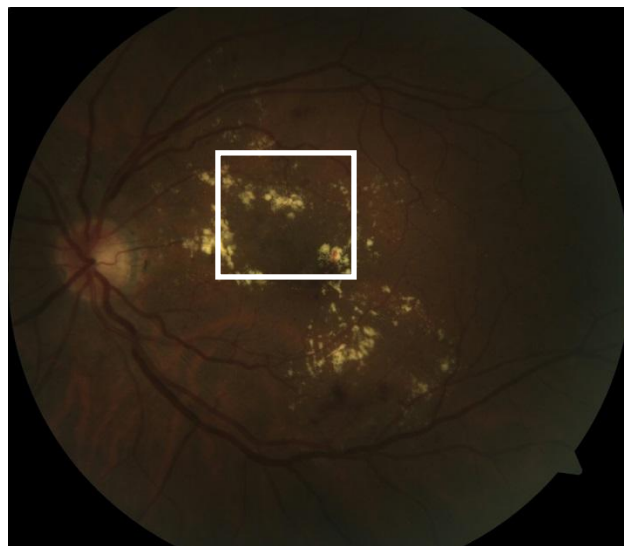
Figure 2.4 Exudates displayed in fundus images.

Cotton wool spots (or soft exudates) are micro infarctions caused by the lack of blood supply to the nerve fibre layer. They appear as yellowish/white structures with blurred edges. Cotton wool spots by themselves do not cause visual difficulties, but they are highly correlated with conditions that affect the retina circulation such as diabetic retinopathy [25].

Retinal hemorrhages are loss of blood from the vasculature. They appear as red structures of variable shape in the fundus image. Their shape can be correlated with the depth in the retina. They are more serious because they are associated with progression of diabetic retinopathy. They often happen because of formation of new fragile blood vessels.

Drusen are yellow deposits of extracellular material below the retina. They are a sign of macular degeneration. Since they are below the retina, they are sometimes not obvious in a fundus image, especially when only few of them are present.

When the blood pressure increases, vessels may increase in length and thicken their walls. Neovascularization is another vascular abnormality due to the lack of oxygen to an area of the retina. These vessels are weaker than normal and are much more likely to create hemorrhages or to leak liquid or proteins [25].

2.3   Diabetic Macular Edema

Diabetic macular edema (DME) is a disease which appears as a complication of DR. It causes vision loss and blindness. In general terms, DME is defined as swelling of the retina in diabetic patients. Actually it is result of the leakage of fluid within the central macula. This leakage comes from microaneurysms that form as the result of damage caused by high blood sugar levels. Figure 2.5 illustrated DME with retinal properties.

The presence of clinically significant DME is an important factor for the onset of laser treatment. One of the specific characteristic of DME is seen as thickening of the retina of the eye. The amount of thickening of the retina cannot be detected directly from a single two dimensional image, because the image lacks in-depth knowledge.

For this reason, ophthalmologists can conclude the presence of the fluid which causes the retina thickening from fundus's photos. This structure associated with the presence of fluid is called an exudate. They are seen as bright structures in the image and they have well defined edges and variable shapes [25].
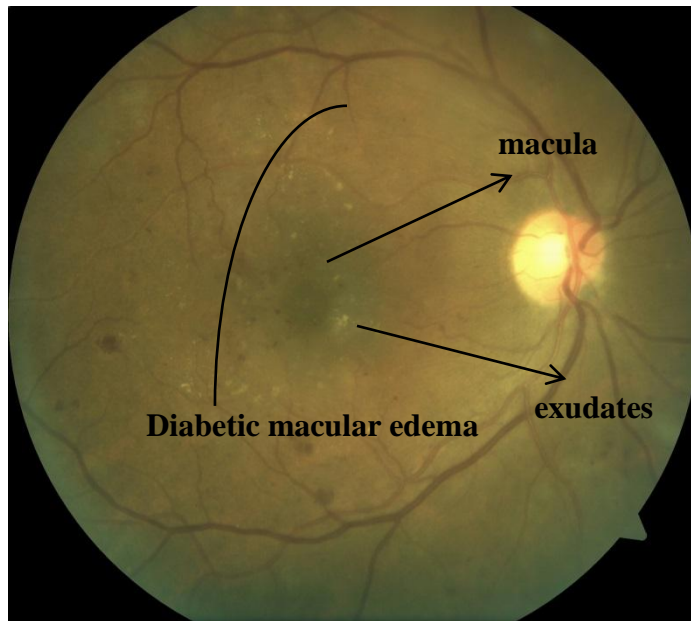
Figure 2.5 Diabetic macular edema and macula, exudates illustrated in a color fundus photography image.

Early Treatment Diabetic Retinopathy Study Research Group (ETDRS) should be treated the patient's retina immediately when degree of DME is clinically significant. This research group is supported by National Eye Institute. It is based on a multicenter and randomized clinical studies. Its research focused on the management of treatment with NPDR and early PDR patients [26].

The ETDRS identify the criteria for which cases must be treated [27]:

The first criterion is a significant retinal thickening within 500 mm distance from the center of the macula.

The second criterion is exudation within 500 mm distance from the center of the macula with retinal thickening in the bordering retina.

The third criterion is a retinal thickened area by the size of at least one papilla diameter within the distance of one papilla diameter from the center of the macula. The papilla roughly corresponds to the visible area covered by the Optic Nerve in a fundus image [25].

If any of the following criterion is satisfied with the patient, then this patient is required to be treated according to ETDRS.

2.4 Diagnosis Methods for Diabetic Retinopathy and Diabetic Macular Edema

There are few types of DR examination methods but mainly ophthalmoscopy (indirect and direct), fluorescein angiogram and fundus photography are used [1].

Direct ophthalmoscopy is the examination method performs by the specialist in a dark room. A beam of light is shined through the pupil using ophthalmoscope. This allows the specialist to view the back of the eyeball.

Indirect ophthalmoscopy is performed with a head or spectacles-mounted source of illumination positioned in the middle of the forehead [28]. A bright light is shined into the eye using the instrument on the forehead. The condensing lens is placed on the eye to intercept the fundus reflex. A real and inverted image of the fundus will form between the examiner and the patient [28].

Fluorescein angiography is a test which allows the blood vessels in the back of the eye. It can be photographed as a fluorescent dye is injected into the bloodstream via the hand or arm [29]. The pupils will be dilated with eye drops and the yellow fluorescent dye is injected into a vein from the arm [29]. It is used to examine the blood circulation of the retina using the dye tracing method.

Figure 2.6 Zeiss Visucam PRO fundus camera is used in this publicly available dataset [30].

Fundus photography is the usage of fundus camera to photograph the regions of the vitreous, retina, choroid and optic nerve [31]. Fundus photographs are only considered medically necessary where the results may influence the management of the patient. In general, fundus photography is performed to evaluate abnormalities in the fundus, follow the progress of a disease, plan the treatment for a disease, and assess the therapeutic effect of recent surgery [31]. Figure 2.6 shows an example of fundus camera.

2.5   Treatment Methods for Diabetic Retinopathy and Diabetic Macular Edema

Treatment of DR varies depending on the extent of the disease [32]. During the early stages of DR, no treatment is needed unless macular edema is present. However, for advanced DR such as PDR, surgery is necessary.

Scatter laser treatment performed to treat advanced stage of DR. An ophthalmologist uses a laser to "scatter" many small burns across the retina in the period of scatter laser treatment. This causes the formation of leakage and abnormal blood vessels become smaller [32]. This surgical method is used to reduce vision loss. However, if there exists significant amount of hemorrhages, scatter laser treatment is not suitable.

Another treatment method called as a vitrectomy is performed under either local or general anesthesia. An ophthalmologist makes a tiny incision in the eye and carefully removes the vitreous gel that is clouded with blood. After the vitreous gel is removed from the eye, a clear salt solution is injected to replace the contents [32].

Leakage of fluid from blood vessels can sometimes lead to macular edema, or swelling of the retina. Focal laser treatment is performed to treat macular edema. Several hundred small burns are placed around the macula in order to reduce the amount of fluid build-up in the macula [32].

The other one is called as laser photocoagulation is a powerful beam of light which combined with ophthalmic equipment and lenses, can be focused on the retina [33]. Small bursts of laser are used to seal leaky blood vessels, destroy abnormal blood vessels, seal retinal tears, and destroy abnormal tissue in the back of the eye [33]. This procedure is used to treat DR patients in PDR stage. The main advantage of using this surgical method is the short surgical duration and the patient usually can resume activities immediately.

2.6   Digital Image

Images describe how a parameter changes over a surface. A digital image is defined as a discrete representation, which contains information on the both spatial and intensity. Digital image structure is shown in Figure 2.7. The image is expressed as 40.000 samples which is created in a two dimensional array of 200 columns by 200 rows. Two dimensional signals are numbered in the same way as one-dimensional signals. These rows and columns can be numbered 0 through 199, or 1 through 200. Each sample of the image is described as pixel and it is used as an abbreviation for picture element in imaging jargon.

Each pixel in the Figure 2.8 displayed as a single number between 0 and 255. The value of each pixel is converted into a grayscale, where 0 is black and 255 is white, and the intermediate values are shades of gray in order to display this as a visual image. There is generally a corresponding intensity value used for black and white images (grayscale) varies between 0 (black) to 255 (white) at any given pixel. Gray values for 8 bit images are 2^8, 4096 gray levels for 12 bit images, etc.

Figure 2.7 Grayscale of the image

o	o	o	o	o	o	o	o	o	o
o	o	o	o	o	o	o	o	o	o
o	o	o	o	o	o	o	o	o	o
o	o	o	o	o	o	o	o	o	25
o	o	o	o	o	o	o	o	21	107
o	o	o	o	o	o	o	12	99	131
o	o	o	o	o	o	3	82	128	129
o	o	o	o	o	o	59	128	128	131
o	o	o	o	o	28	120	131	133	132
o	o	o	o	5	94	132	134	135	133
o	o	o	o	51	126	131	133	135	137
o	o	o	12	108	131	132	132	132	128
o	o	o	60	132	133	130	122	129	139

Figure 2.8 Pixel value of small box of the grayscale image

256 gray levels (quantization levels) are used for image processing in a widespread way. In addition to this, these gray levels correspond to a single byte per pixel in image. There are many reasons why using this level. First, a single byte is more convenient to choose for data management because this provides how computers typically store data. Second, the large amount of pixels in an image makes up a certain degree for a limited number of quantization steps. Third, the most important one is, a brightness step size of 1/256, which is expressed as 0.39% is smaller than the eye can also be sensed. An image provided by a human observer will not be got better by using the greater than 256 levels.

Color is generated by adding digital images using three numbers for each pixel. It represents the intensity of the digital images using three primary colors: red, green and blue. RGB images require a three-dimensional array in order to transfer the extra color information in RGB images.

In Figure 2.9, shows red channel which represents first plane, green channel which represents second plane and blue channel which represents third plane of the fundus image [34].
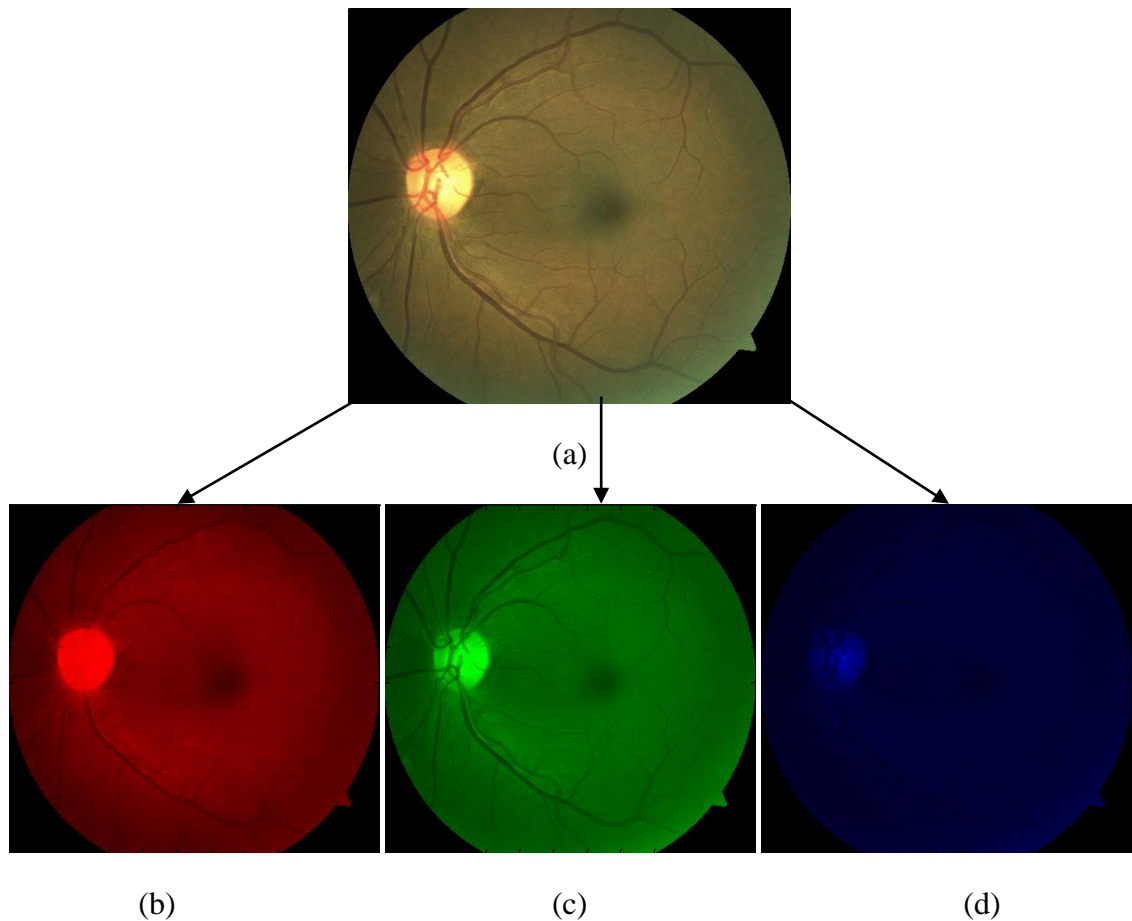
Figure 2.9 Red, Green and Blue channel of the image: Original image is shown in (a), red channel of the original image is shown in (b), green channel of the original image is shown in (c) and blue channel of the original image is shown in (d).

The green channel is used to enlarge the contrast for fundus image analysis. This channel increases contrast between the back-ground and features, such as blood vessels and hemorrhages [35].

But many image processing and measurement tools designed to operate on gray-scale image. Therefore this may need to be extracted from an RGB color image. Indexed images generated by matrices or using predefine a limited set of combinations of RGB values defined as color maps. Then, the pixel value simply refers to the closest combination from the color map instead of each point in the digital image defining RGB levels individually. Thanks to this, the time taken for the storage of the image is reduced. A binary image is composed of only black and white pixels. The image is form of a binary array, generally consisting of 0's and 1's. Images of any type may be converted to this format for processing or analysis.

Thanks to a mixture of these three colors, in all possible colors can be detected by the human eye. A single byte is used to store each of the color intensities many times. As a result of this, a total of 256*256*256 = 16.8 million different colors provide the image to be captured. The aim of the engineering can summarize as analyzing a two-dimensional signal by using the human visual system as a tool and for this aim black and white images are sufficient [34].

2.7   Medical Image Processing

Digital image processing points to process digital images by means of a digital computer. Digital image processing is a discipline that uses the image during input and output of the process. In addition, it encompasses processes that extract features from images, up to and including the recognition of individual objects. If it is applied in medical field, it is called as a medical image processing [36]. Medical image processing allows the use of much more complex algorithms, and hence, can offer both more sophisticated performance at simple tasks, and the implementation of methods which would be impossible by analog means [37].

MATLAB software program was used for implementation of image processing method in this thesis. The name MATLAB means matrix laboratory. MATLAB is an interactive system whereas C or Fortran is a scalar non-interactive language. In a fraction of the time it would take to write a program in C or Fortran. Fundamental data element of MATLAB is an array that does not require dimensioning. This allows formulating solutions to many technical computing problems, especially those including matrix representations [36].

MATLAB has many set of tools available for various operations. The main toolbox used for this thesis is Image Processing Toolbox. It consists of a wide range of image processing functions to analysis, enhance or perform on the images [38].

2.7.1   Mathematical Morphology

Morphology is a wide range of image processing operations involving process images according to shapes. Mathematical morphology mostly deals with the mathematical theory of describing shapes using sets and it can be used for preprocessing like noise filtering, shape simplification; enhancing object structure like skeletonization, convex hull; segmentation like watershed; quantitative description like area, perimeter [36].

Morphological operations are applied to an input image with a structuring element and an output image, which is the same size as the input image occurs. Morphological operation is related to the value of each pixel in the output image which is based on a comparison of the corresponding pixel in the input image with its neighbors. Morphological operation that is sensitive to specific shapes in the input image can be produced by changing the size and shape of the neighborhood. There are many types of morphological operations such as dilation, erosion, opening and closing.

Structuring element is used for the purpose of image processing. The size and shape of structuring element determines how much number of pixels added or removed from the objects in an image.

2.7.1.1 Dilation and Erosion

In the morphological dilation and erosion operations, the state of any given pixel in the output image is determined by applying a rule to the corresponding pixel and its neighbors in the input image. The rule used to process the pixels defines the operation as dilation or erosion [39].

Dilation is an operation that grows or thickens objects in a binary image [36]. Figure 2.10 illustrates the dilation process. In dilation the value of the output pixel is the maximum value of all the pixels in the input pixel's neighborhood. In a binary image, if any of the pixels is set to the value 1, the output pixel is set to 1.

To dilate an image, imdilate function is used in MATLAB. The imdilate function accepts two primary arguments:

(i)   The input image to be processed (grayscale, binary, or packed binary image).

(ii)   A structuring element object, returned by the strel function, or a binary matrix defining the neighborhood of a structuring element [39].

Figure 2.10 Left side of the image is original image; right side of the image is dilated image with certain disk structuring element.

Erosion shrinks or thins objects in a binary image. Figure 2.11 illustrates the erosion process. The value of the output pixel is the minimum value of all the pixels in the input pixel's neighborhood. In a binary image, if any of the pixels is set to 0, the output pixel is set to 0.

To erode an image, imerode function is used in MATLAB. The imerode function accepts two primary arguments:

(i)   The input image to be processed (grayscale, binary, or packed binary image).

(ii)   A structuring element object, returned by the strel function, or a binary matrix defining the neighborhood of a structuring element [39].

Figure 2.11 Left side of the image is original image; right side of the image is eroded image with certain disk structuring element.

2.7.1.2 Opening and Closing

The process of a morphological opening of an image is erosion followed by dilation, using the same structuring element for both operations. Figure 2.12 illustrates the morphological opening process. Morphological opening is used to remove small objects from an image while preserving the shape and size of larger objects in the image [39]. It removes completely regions of an object that cannot contain the structuring element, smooth object contours, breaks thin connections, and removes thin protusions [36].

Figure 2.12 Left side of the image is original image; right side of the image is opened image.

The morphological closing of an image is the reverse of opening. It consists of dilation followed by erosion with the same structuring element. Figure 2.13 illustrates the morphological closing process. Like opening, morphological closing tends to smooth the contours of objects. Unlike opening, however, it generally joins narrow breaks, fills long thin gulfs, and fills holes smaller than the structuring element [39].

Figure 2.13 Left side of the image is original image; right side of the image is closed image.

2.7.1.3 Structuring Element

A structuring element (SE) is a binary morphology that is used to probe the image. It is a matrix consisting of only 0's and 1's that can have any arbitrary shape and size. The pixels with values of 1 define the neighborhood [39]. There are two types of SE, two-dimensional or flat SE usually consists of origin, radius and approximation N value. Three-dimensional or non-flat SE usually consists of radius (x-y planes), height and approximation N value. There are different types of SE shapes but in this thesis, disk shaped and ball shaped SE are used.

Disk shaped SE, *SE = strel('disk', R, N)* creates a flat, disk shaped structuring element, where R specifies the radius. R must be a nonnegative integer and N must be 0, 4, 6, or 8 [40]. Figure 2.14 shows a disk shaped SE with radius 3 and its center of origin.

0	0	0	1	0	0	0
0	1	1	1	1	1	0
0	1	1	1	1	1	0
1	1	1	1	1	1	1
0	1	1	1	1	1	0
0	1	1	1	1	1	0
0	0	0	1	0	0	0

R=3

Origin
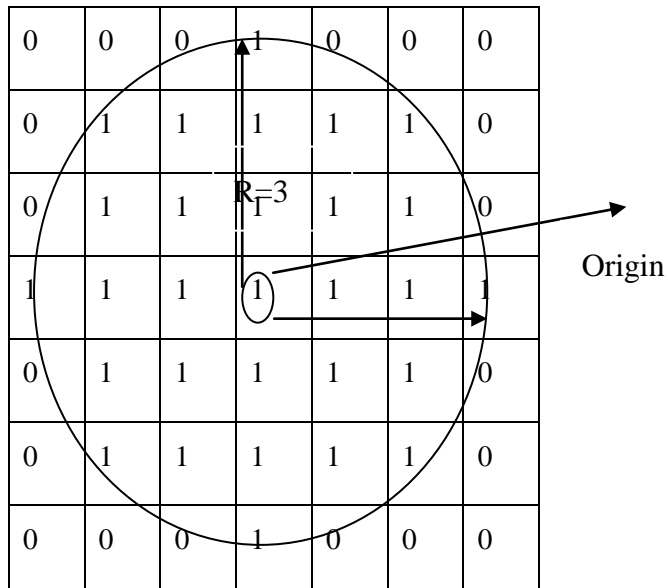
Figure 2.14 Disk shaped structuring element

Ball shaped SE, *SE = strel('ball', R, H, N)* creates a non-flat, ball-shaped structuring element (actually an ellipsoid) whose radius in the X-Y plane is R and whose height is H. Note that R must be a nonnegative integer, H must be a real scalar, and N must be an even nonnegative integer [40]. Figure 2.15 shows a ball shaped SE with x-y axis as radius and z axis as height.

z-axis

height

radius

x-axis

y-axis
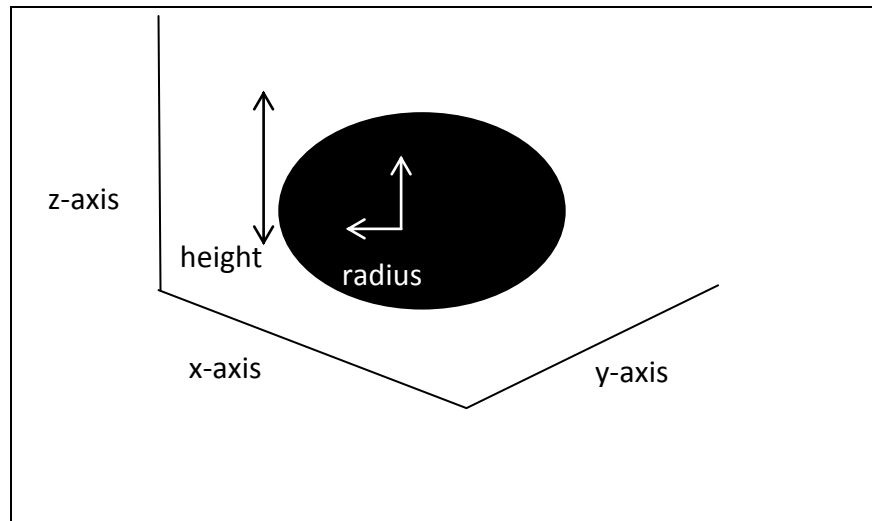
Figure 2.15 Ball shaped structuring element (non-flat ellipsoid)

2.7.2 Circular Hough Transform

Hough transform is a method for estimating the parameters of a shape from its boundary points. Hough proposed a method to detect straight lines in images [41]. The Hough transform is not restricted to detecting straight lines, though that is a common use. It can also be used to find circles, or even generalized to find any shapes. The circle Hough Transform has been implemented to find circles within an image. The circle Hough Transform is almost identical to the Hough Transform for lines, but uses the parametric form for a circle [42]:

$$(x - a)^2 + (y - b)^2 = r^2 \tag{2.1}$$

where (a, b) is the centre of the circle of radius r that passes through (x, y).

To find circles using a Hough transform, you need a three-dimensional accumulator array. Each edge element votes for all the circles that it could lie on, and the 3-D array is searched for peaks that give circle positions and radii. If you happen to know the radius in advance, you only need a 2-D accumulator. Then, every point in (x, y) space corresponds to a surface in (a, b, r) space (we can vary any two of the parameters a, b and r, the third is determined by the equation of the circle Equation 2.1).

The basic method is, thus, modified to use a three-dimensional Hough Space (3-D array) H (a, b, r). All points in it, which satisfy the equation for a circle, are incremented [41].

CHAPTER 3

MATERIALS AND METHODS

3.1   HEI-MED Dataset

In this thesis, we used a publicly available data set called Hamilton Eye Institute Macular Edema Dataset (HEI-MED). This dataset is publicly available to the research community on the website: http://vibot.u-bourgogne.fr/luca/heimed.php.

Hamilton Eye Institute, the Image Science and Machine Vision Group at ORNL in the regions of the Mid-south of the United States of America and Université de Bourgogne in France set a teleophthalmology network. It consists of 169 DME images which stored between 2005 and 2010 [25].

There are some other dataset which include fundus images of the DME patients [43 - 48]. However, these are constituted for different aims such as DR diagnosis, vessel segmentation, and microaneurysm / hemorrhages localization. In literature, there exists one data set which consists of only exudates images but this one do not contain fundus image from different ethnic. Due to the pigmentation of the human retina is significantly variable between different ethnic groups, images from different ethnics is important for exudates segmentation. The HEI-MED dataset includes 169 fundus images, so all these images are analyzed for evaluating the performance of three different OD detection methods. The methods did not work well for the 30 fundus images. For this reason, the results for 30 images and 139 images are evaluated different aspect.

There are various reasons for using this dataset. Firstly, HEI-MED actively is used to provide development of new algorithms for the automatic detection of diabetic

retinopathy and associated diseases. A publicly available dataset can contribute to the advancement of new techniques. Secondly, available algorithms for the segmentation of exudates and the detection of diabetic macular edema is impossible to be easily compared due to the several authors used independent datasets. For this reason, it makes sense to use a common dataset to make the comparison easier when comparing [25].

The dataset consists of high-quality compressed 169 Jpeg images. Images have certain characteristics. All the images had enough quality, no patient is duplicated, a reasonable mixture of ethnicities and disease stratification is represented. Table 3.1 shows the distributions of the ethnicity, DME diagnosis, and Elliptical Local Vasculature Density features (ELVD) quality [3], diabetes type and patients' age in the dataset.

Table 3.1 Demographic Data of HEI-MED

Ethnicity			
African American	104(62%)	Hispanic	19(11%)
Caucasian	42(25%)	Unknown	4(2%)
DME diagnosis			
Negative	115(68%)	Positive	54(32%)
Patients age			
Age<26	5(3%)	26≤age<43	20(12%)
43≤age<61	105(62%)	Age≥61	39(23%)
Diabetes Type			
Type 1	160(95%)	Type 2	6(3.5%)
Unknown	3(1.5%)		
ELVD quality metric			
Poor	14(8%)	Good	31(18%)
Excellent	124(74%)		

Each image of the dataset was manually segmented by Dr. Edward Chaum (an expert ophthalmologist from HEI). He identified all the exudation areas and other bright lesions such as cotton wool spots, drusens or clearly visible fluid occurring on the fundus [25]. Also he divided all 169 images into two categories as hard or non hard exudates.

The ELVD quality metric is an algorithm to automatically detect the quality of a fundus image. In addition to the images and the ground truth, other anonymous clinical metadata about the patients, the optic nerve manually identified location, the machine segmented vasculature (employing the method of Zana and Klein [49]) and a MATLAB class to seamlessly access all the data and metadata without having to deal with the internal format of the files are provided [50].

HEI-MED dataset has several advantages over existing datasets as described below:

(i)   diverse ethnicity,

(ii)   image consistency,

(iii)   quality assessment,

(iv)   metadata.

The telemedicine network is employed the clinics which are especially located in the Mid-South of the USA, where the ethnic groups are not homogeneous and where retinal pigmentation contains the spectrum information generally found in diverse populations. The appearance of the retinal varies greatly depending on the pigmentation of the retinal pigment epithelium, for this reason it is important to focus on diverse ethnicity aspect. The retinal pigment epithelium is correlated to the ethnic group and eye color. Depending on this pigmentation, lesions or other type of structures become more or less evident. Because of this, it makes the development of lesion segmentation and diagnosis algorithms that work on a broad spectrum of patients more challenging [25] shown in Figure 3.1 and 3.2.
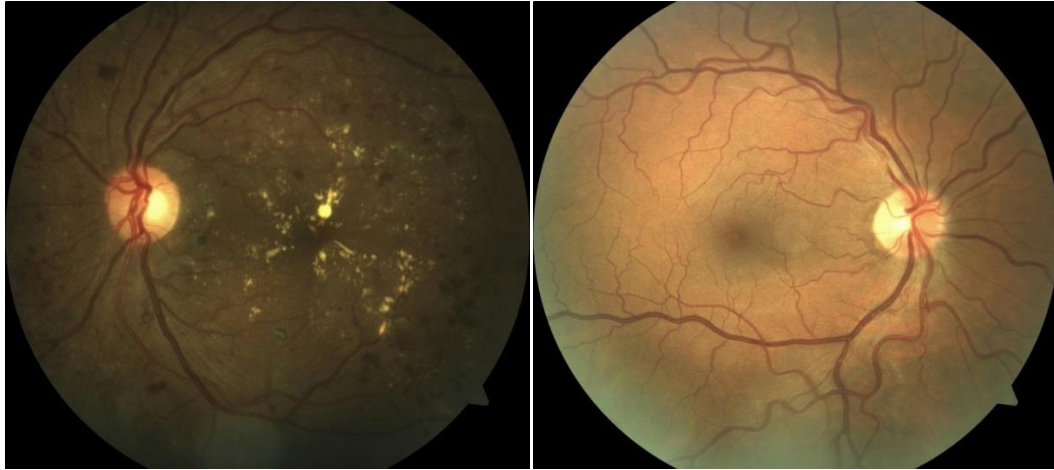
Figure 3.1 Left side of the image is Hispanic Patient showing clear exudates; right side is Caucasian patient without sign of DME.
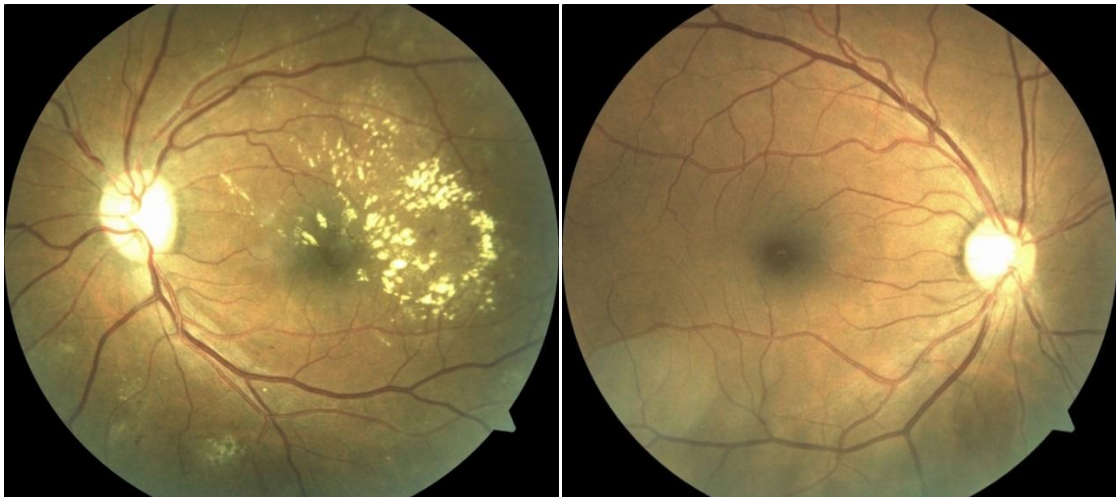
Figure 3.2 Left side of the image is African patient showing clear exudates; right side is African patient without sign of DME.

All the images are captured with the Zeiss Visucam PRO fundus camera, at a resolution of 2196*1958 pixels and with a 45º Field of View.

Every time an image is captured the automatic quality assessment algorithm is run and the result is shown to camera operators, giving them the chance of taking a new image if required. Thus each image in the dataset has an ELVD quality value stored for comparison.

All the images have a manually generated location of the Optic Nerve information [25]. In this thesis, we used this information for comparing OD center coordinates obtained by three methods.

3.2   Automatic OD-Detection Methods

In the literature, several different techniques have been implemented to automatically detect the OD. The Figure 3.3 illustrates general steps in these methods that determine the OD.

```
┌─────────────────┐      ┌─────────────────┐      ┌─────────────────┐
│  Preprocessing of │  ⇒   │ Image processing │  ⇒   │ Optic disc detection │
│      Image       │      │    operation     │      │                  │
└─────────────────┘      └─────────────────┘      └─────────────────┘
```
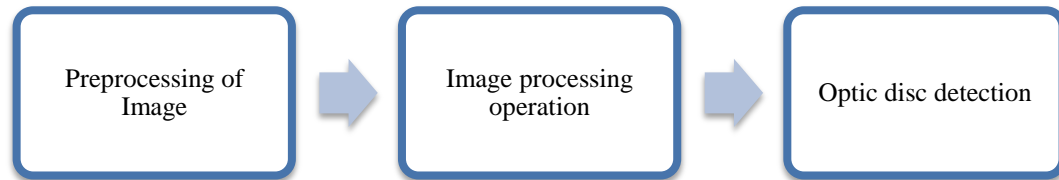
Figure 3.3 The process of detecting optic disc

In the thesis, three different techniques were applied to the fundus image. The detailed of these techniques are explained below. First method is based on Hough Transform. Second and third methods are based on mathematical morphology. Third method is also proposed as a new method.

3.2.1.   Method I Based on Hough Transform

Figure 3.4 shows the system block diagram of optic disc detection using method I. The detailed steps are explained below.

Figure 3.4 System block diagram for detecting optic disc.

The shape of the OD is almost circular in the fundus images. Therefore, we are looking for circular structure on the images in order to locate the potential optic disk region.

To identify the circles in an image, first of all binary edge of the image should be determined. Figure 3.5 is an example of binary edge map of original image. For this aim, images are converted into grayscale level.
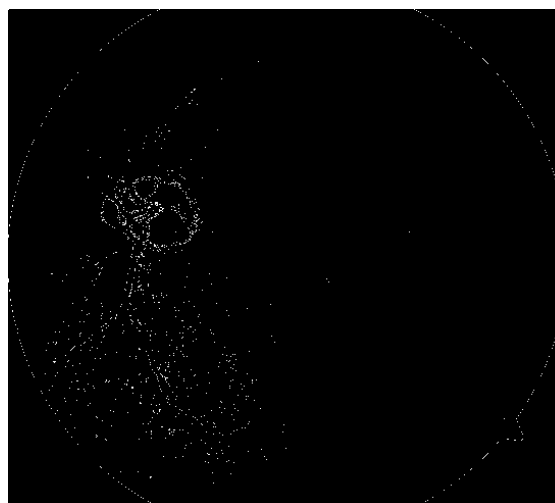
Figure 3.5 Binary edge map of original image

Then Hough space is constituted for a circular parameter which gets through every edge point shown in Figure 3.6. For Hough space, the values of a and b can set to compute r value using Equation 2.1. According to new r value the position knowledge should update and these process are repeated to get most accurate values for a and b within the range of interest.
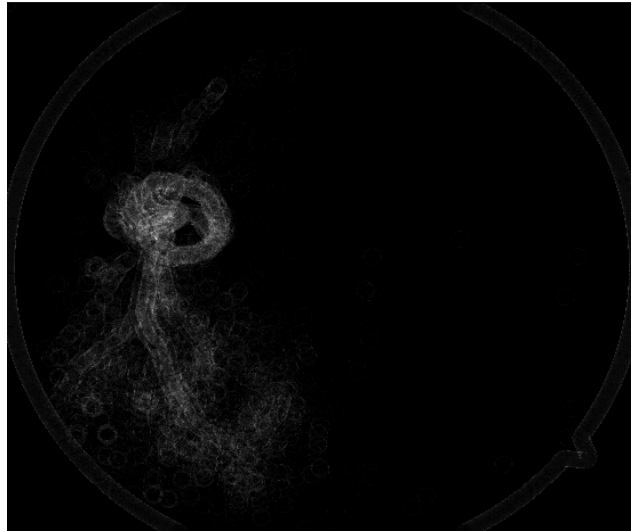
Figure 3.6 Hough space of binary image

Lastly the maximum point of Hough space is determined as the best center of the OD. Thus, we find the OD center of original image which is shown in Figure 3.7.

Figure 3.7 Optic disc center marked by Method I

3.2.2. Method II Based on Mathematical Morphology

Method II: Figure 3.8 shows the system block diagram of optic disc detection by method II. The detailed steps are explained below.

Firstly, as part of the image preprocessing step, we adjust image intensity values. In Figure 3.9 shows an example of adjusted image. Some intensity values were tried and most suitable values for images were selected experimentally.

Figure 3.9 Adjusted image

```
                    ┌─────────────────────────┐
                   /      Original image        /
                  └─────────────────────────┘
                               │
                               ▼
              ┌──────────────────────────────┐
              │    Preprocessing of the image   │
              └──────────────────────────────┘
                               │
                               ▼
              ┌──────────────────────────────────┐
              │ Gray channel of the adjusted image is selected │
              └──────────────────────────────────┘
                               │
                               ▼
              ┌──────────────────────────────┐
              │     Morphological opening        │
              └──────────────────────────────┘
                               │
                               ▼
              ┌──────────────────────────────┐
              │   Construct the optic disc mask  │◄────┐
              └──────────────────────────────┘      │
                               │                          │
                               ▼                          │
              ┌──────────────────────────────┐      │
              │  Scan the fundus image using OD mask │   │
              └──────────────────────────────┘      │
                               │                          │
                               ▼                          │
                        ◇ Center (OD mask) =              │
                          Max(opened image) ◇─────────────┘
                               │
                               │ Y
                               ▼
              ┌──────────────────────────────┐
              │         OD detection             │
              └──────────────────────────────┘
```
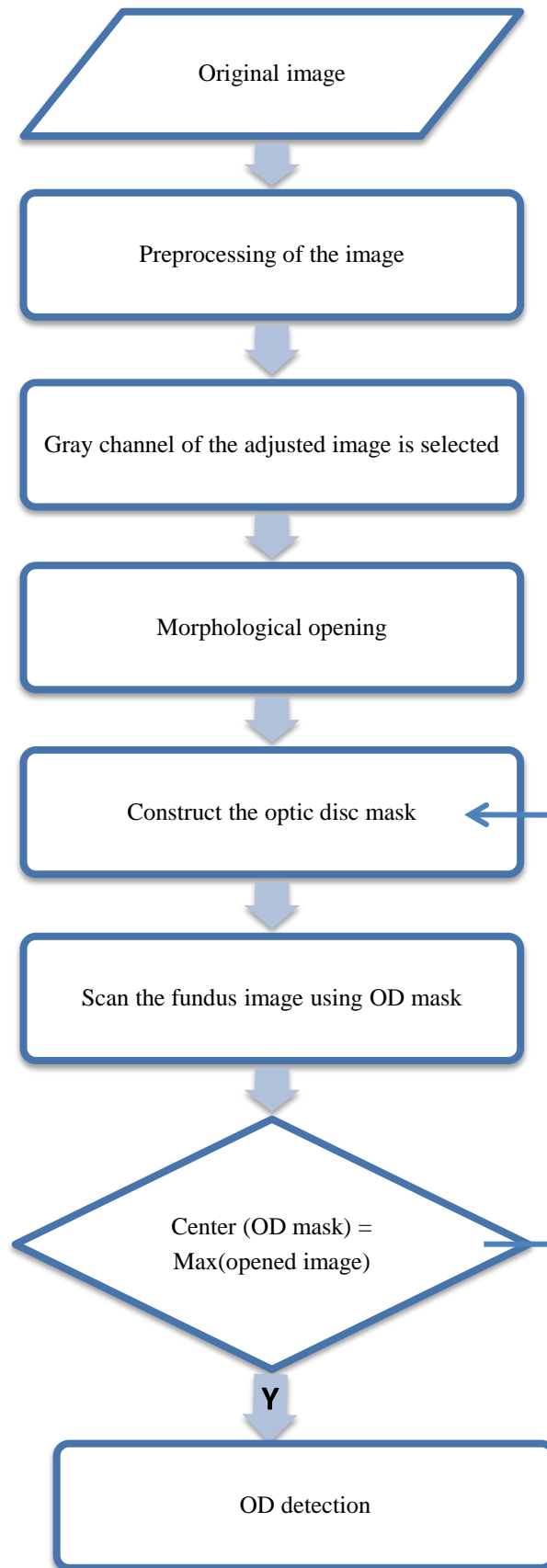
Figure 3.8 System block diagram for detecting optic disc

The OD is defined as a group of bright spots, because of the method which finds the OD using loops and locating the largest value is not appropriate. This would indicate that only a single point and most probably to be on the side of the OD. The location of the optical disc is detected by the brightest point(s) on the gray-scale image which is shown in Figure 3.10. Grayscale image is known to be more effective for the detection of OD. Before locating the largest value, first of all find the max value for each of the images [38]. The coordinates of each bright spots are then determined and the median is used if there is more than one point.

Figure 3.10 Gray-scale of the image

OD is usually the maximum value of grayscale image. After locating the optical disk, a mask is constructed in Figure 3.11. A mask is required during the exudates classification process since it has similar attributes to the exudates in terms of color.

Figure 3.11 Optical disc mask

A simple square mask created using loops could be easy but this would have caused the error when the optical disk is close to the border of the image. Therefore, the circular mask instead of simple square mask is used [38]. Lastly the result of the masking process with circular mask is defined as OD. Thus, OD center becomes the center of the mask in Figure 3.12.

Figure 3.12 Optical disc detected by method II

3.2.3.   Method III Based on Mathematical Morphology

Figure 3.13 shows the system block diagram of optic disc detection by method III. The detailed steps are explained below.

```
                    ┌─────────────────────────┐
                   ╱      Original image      ╱
                  └─────────────────────────┘
                              │
                              ▼
                 ┌─────────────────────────────┐
                 │  Resizing the original image │
                 └─────────────────────────────┘
                              │
                              ▼
                 ┌─────────────────────────────┐
                 │  Red component of the resized │
                 │      image is selected        │
                 └─────────────────────────────┘
                              │
                              ▼
                 ┌─────────────────────────────┐
                 │  Gaussian filter is performed │
                 └─────────────────────────────┘
                              │
                              ▼
                 ┌─────────────────────────────┐
                 │ Morphological opening using disk SE │
                 └─────────────────────────────┘
                              │
                              ▼
                 ┌─────────────────────────────┐
                 │     Background detection      │
                 └─────────────────────────────┘
                              │
                              ▼
                 ┌─────────────────────────────┐
                 │ Subtracting background from the │
                 │        resized image          │
                 └─────────────────────────────┘
                              │
                              ▼
                 ┌─────────────────────────────┐
                 │ Morphological opening using ball │
                 │              SE               │
                 └─────────────────────────────┘
                              │
                              ▼
                 ┌─────────────────────────────┐
                 │       Max(opened image)       │
                 └─────────────────────────────┘
                              │
                              ▼
                 ┌─────────────────────────────┐
                 │        Optic disc             │
                 │        detection              │
                 └─────────────────────────────┘
```
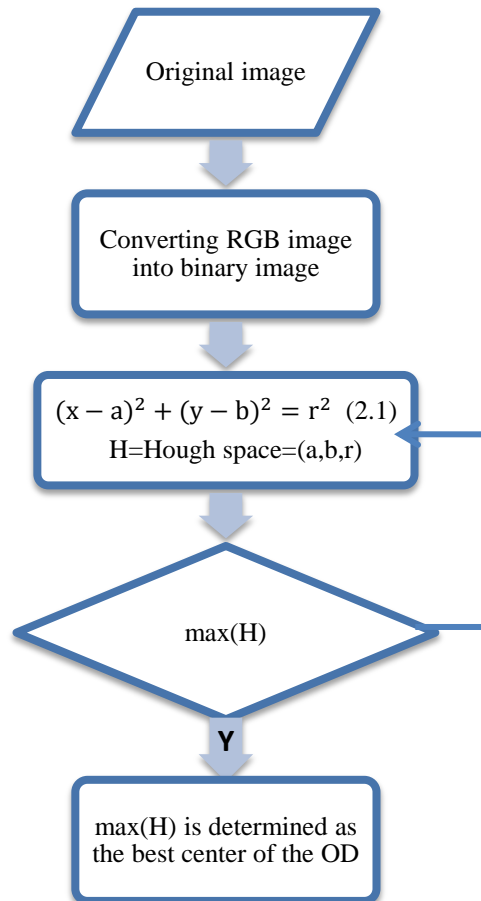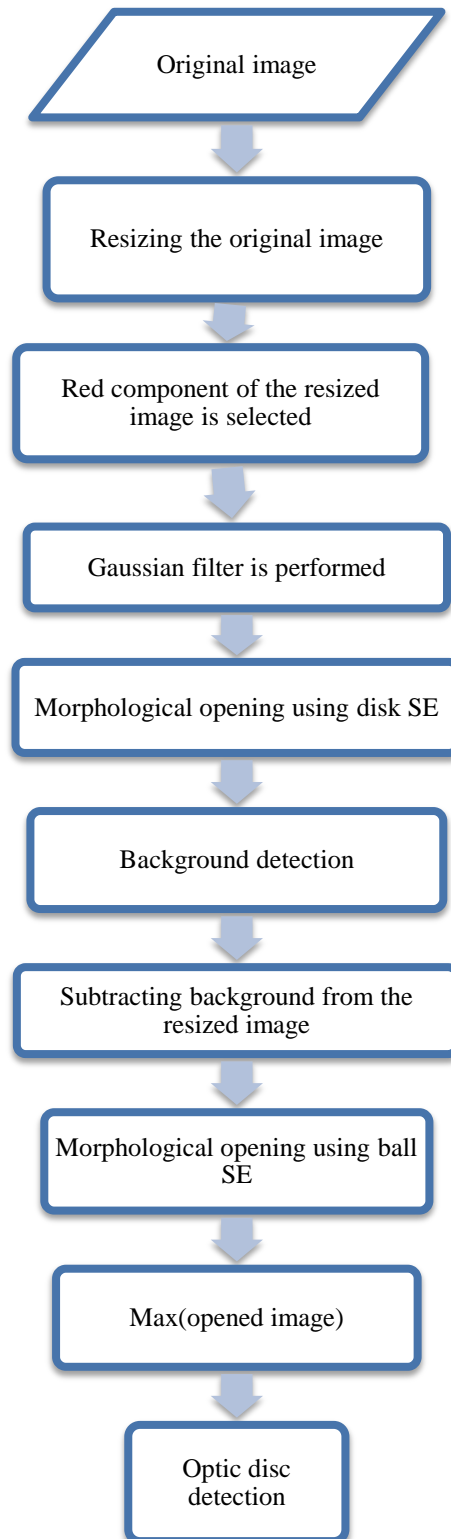
Figure 3.13 System block diagram for detecting optic disc.

In our method, we proposed a key-lock principle based approach to detect OD center.
The Fundus image's size is too large. This means that it takes long computational time.
For reducing this computational time, the fundus image shown in Figure 3.14 (a) is first

preprocessed to standardize its size to 490*549. Red channel of color image is extracted for processes, shown in Figure 3.14 (b) since it is found to be the most successful.
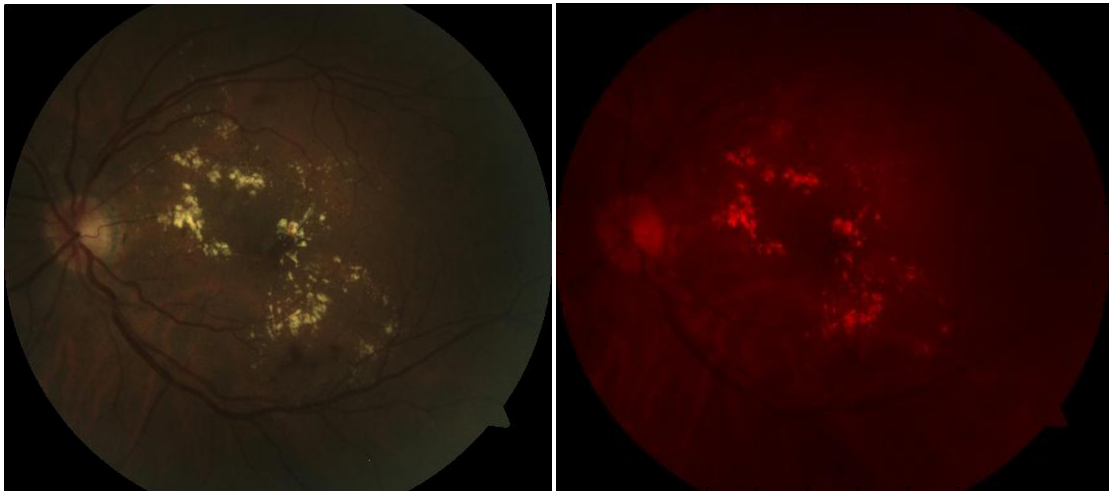
(a)   (b)

Figure 3.14 (a) Original image, (b) Red channel of the image

Then, we applied a Gaussian low pass filter to eliminate high frequency noise and JPEG conversion artifacts caused by ophthalmoscope device itself. In Figure 3.15, illustrates an example of the filtered image.
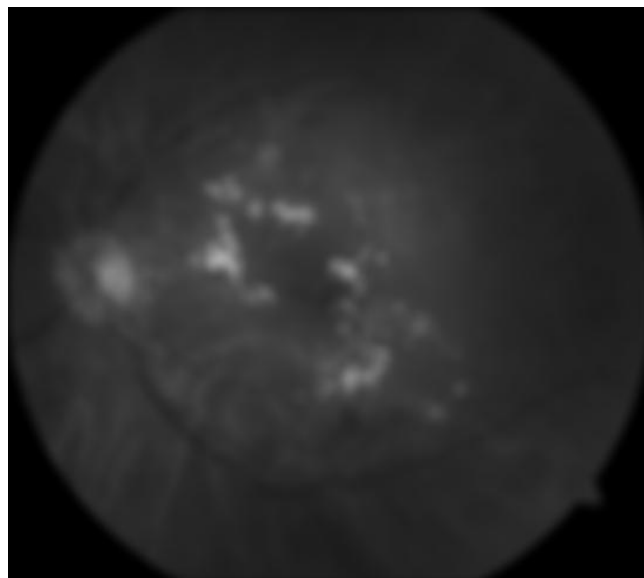
Figure 3.15 Filtered image

After the elimination of high frequency noise, we did an elimination of low frequency background illumination by subtracting the morphologically opened form of the image with a disk shaped flat Structuring Element which has a diameter 40 larger than OD. This opened image is constructed background of the image. This stage is important

because of the large illumination differences between images. Then we subtracted background from the resized image shown in Figure 3.16 (a). As a result of this, illumination of the image becomes corrected shown in Figure 3.16 (b).

(a)   (b)
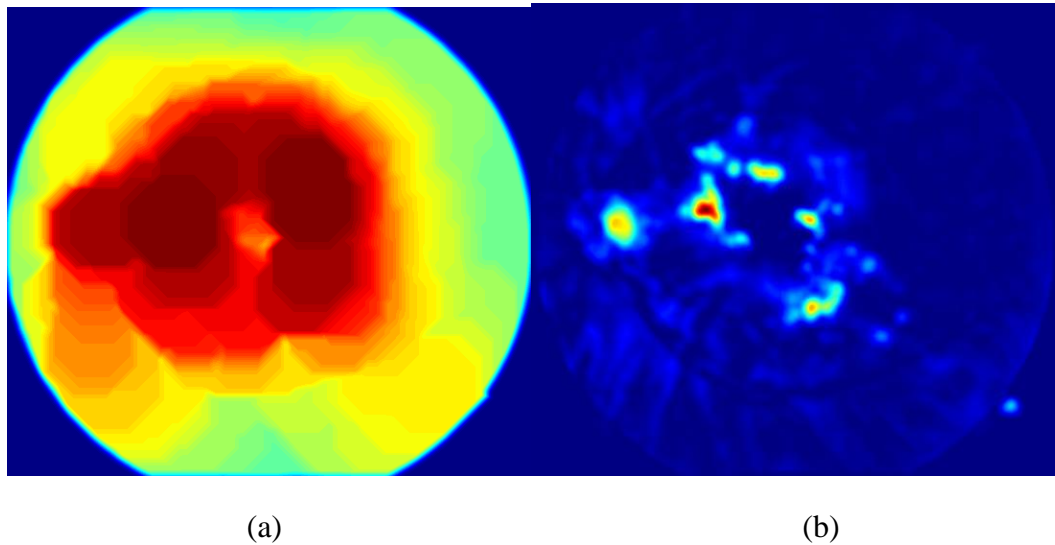
Figure 3.16 (a) Background of the image, (b) Illumination of image is corrected.

Following the image adjustment stages, we formed a non-flat, ellipsoid-shaped SE which has radius 75 and height 300 shown in Figure 3.17.

Dimensions of the SE are selected so that it fits into OD. Adjusted images are opened with this SE.
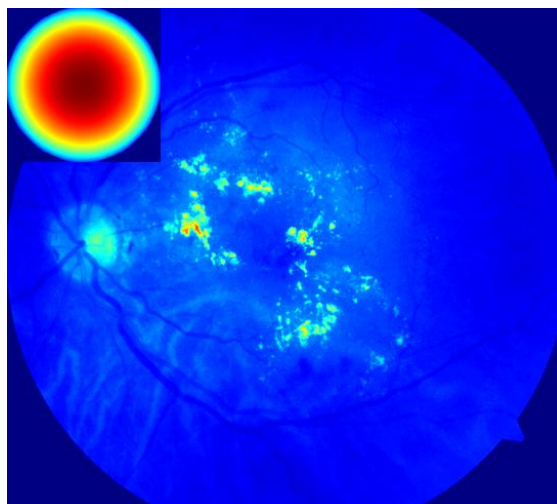
Figure 3.17 Ball shaped structuring element shown in left corner of the red channel of the image

This provided us to eliminate vessels and exudates which SE does not fit into, while keeping the OD untouched. In Figure 3.18 (a) illustrates an example of opened image. By this operation, we obtained a new image. Finally we defined the centroid of the

maximums of this image as a center point of OD. Figure 3.18 (b) shows the maximum of the opened image.

Then, Figure 3.18 (c) shows the final of the image which is marked with OD center.
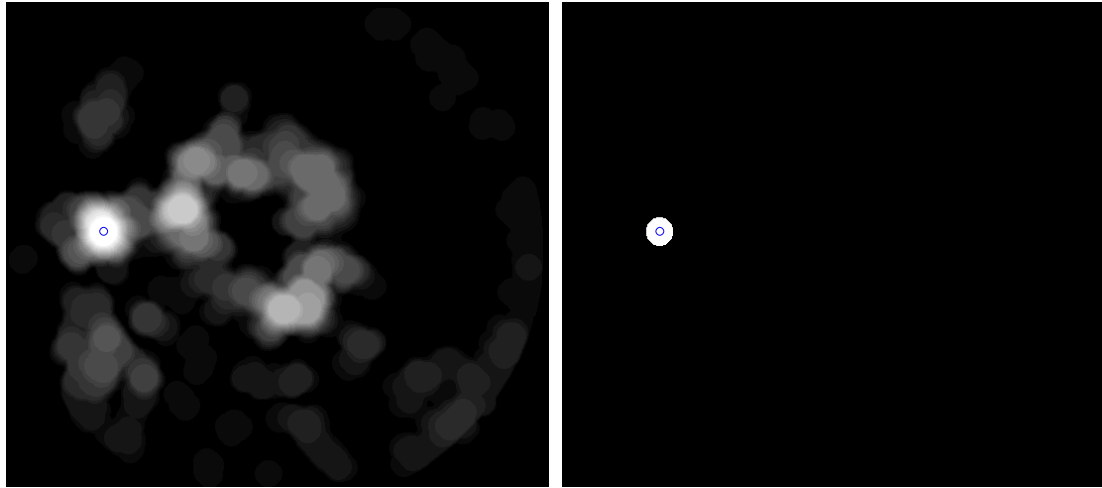
(a)   (b)
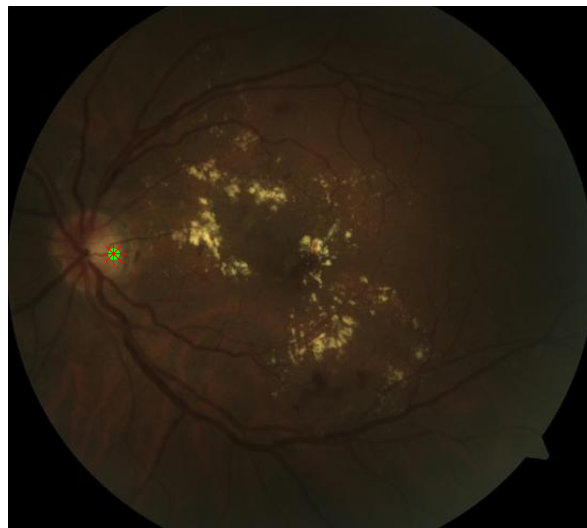
(c)

Figure 3.18 (a) Opened image with specified SE, (b) Maximum of opened image,

(c) Final image.

CHAPTER 4

RESULTS

In this thesis the performance of the three different OD detection methods in fundus images was evaluated and compared based on the determining the center of OD with regard to the manually segmented optic disc center.

For this aim, 169 hard exudates and non-hard exudates retinal images were used from a publicly available dataset which consist of DME fundus images. The OD center coordinates which detected by three methods were defined as [x, y] and the manually segmented were defined as [x_0, y_0]. Results for [x, y] and [x_0, y_0] from 45 hard exudates images are given in Table A.1 and results for [x, y] and [x_0, y_0] from 94 non-hard exudates images are given in Table A.2 as APPENDIX A and results for [x, y] and [x_0, y_0] from rest 30 images are given in Table A.3.

The difference between the [x, y] and [x_0, y_0] would be the error (R) and is calculated by Equation 4.1.

$$R = \sqrt{(x_o - x)^2 + (y_o - y^2)} \tag{4.1}$$

R values are computed for 169 hard exudates and non-hard exudates retinal images individually. OD center detection performance is tested by calculating the mean (μ) and standard deviation (σ) of the R values. To compare μ and σ values for three methods from hard exudates images are given in Table 4.1.

As can be seen from the Table 4.1, μ value of method I is 448.1708, method II is 161.4919 and method III is **31.0201** and σ value of method I is 440.4605, method II is

393.2321 and method III is **23.5801** . As a result of this, method III has the smallest error in hard exudates images.

Table 4.1 Performance evaluations of methods from hard exudates images

	Method I	Method II	**Method III**
Mean(R)	448.1708	161.4919	**31.0201**
Standard dev. (R)	440.4605	393.2321	**23.5801**
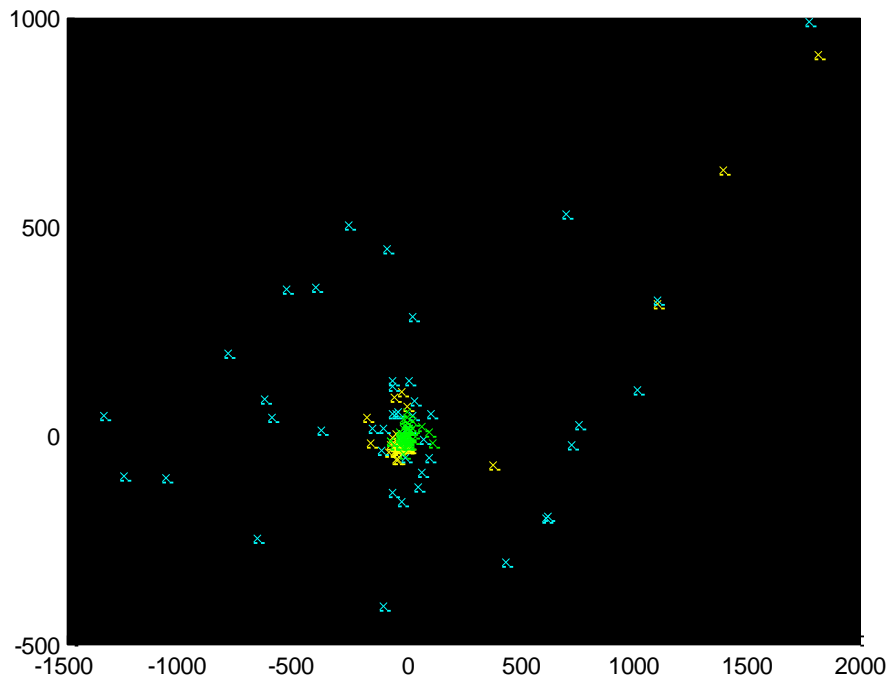
Figure 4.1 Distribution of R values for three different methods in hard exudates images: cyan cross line (×) is used for method I, yellow cross line (×) is used for method II and green cross line (×) is used for method III.

As can be seen from the Figure 4.1, R values of method III are almost zero in hard exudates images. R values of other methods have a scattered distribution. For this reason, method III is the best choice for OD detection in hard exudates images.

To compare μ and σ values for three methods from non-hard exudates images are given in Table 4.2. As can be seen from the Table 4.2, μ value of method I is 233.1443, method II is 121.2222 and method III is **38.1534** and σ value of method I is 282.7639,

method II is 306.0203 and method III is **27.3337**. As a result of this, method III has the smallest error in non-hard exudates images.

Table 4.2 Performance evaluations of methods from non-hard exudates images

	Method I	Method II	**Method III**
Mean(R)	233.1443	121.2222	**38.1534**
Standard dev. (R)	282.7639	306.0203	**27.3337**
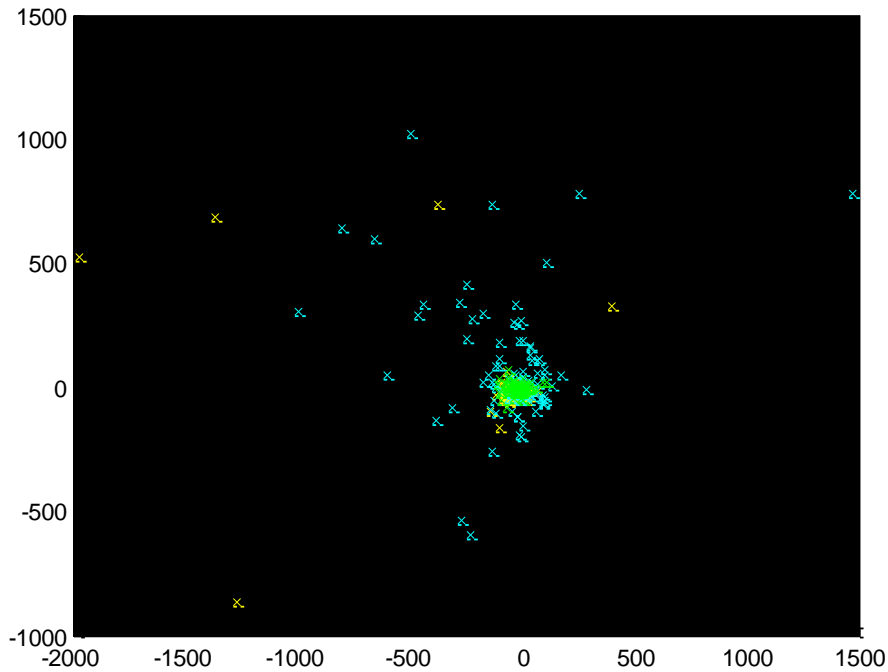
Figure 4.2 Distribution of R values for three different methods in non-hard exudates images: cyan cross line (×) is used for method I, yellow cross line (×) is used for method II and green cross line (×) is used for method III.

As can be seen from the Figure 4.2, R values of method III are almost zero in non-hard exudates images. R values of other methods have a scattered distribution. For this reason, method III is the best choice for OD detection in non-hard exudates images.

And then the obtained results for the rest of 30 fundus images are given in Table A.3 as APPENDIX A.

To compare the three methods from the rest 30 images μ and σ values for R values are given in Table 4.3.

Table 4.3 Performance evaluations of methods from the rest of 30 fundus images

	Method I	Method II	Method III
Mean(R)	272.0310	177.4335	670.8763
Standard dev. (R)	256.7933	315.3570	382.3961

As can be seen from the Table 4.3, μ value and σ value of all three methods are too large. Any method is not a good choice to detect OD center. In other words, all methods cannot detect OD center correctly for the rest of 30 fundus images. For this reason, the rest image excluded from analysis.

DISCUSSION AND RECOMMENDATIONS

As can be seen from the results, method I is not suitable method to find OD center in two aspects according to the rest of the methods. Firstly, method I is used the shape as a feature to decide an OD. However hard exudates parts of the fundus image have similar shape with OD and this properties of the hard exudates cause wrongly detection of the OD center. In Figure 4.1 can be summarized this effect. Other one is about computational time. To detect the circular shape we need to find the edge of the shape and this process use more complex mathematical equations than other methods. In addition the computational complexity of method I highly depends on the number of edge pixels and it is more for hard exudates image than normal fundus image.

Figure 4.3 A hard exudate image and OD centers. Positive sign (+) is used to show OD center which detected by ophthalmologist and triangle shape (Δ) is used to show method I.

Method II is ineffective to find OD center of fundus images where exudates are brighter than the OD shown in Figure 4.2. This method also depends on brightest part of the image and the size of mask. Therefore, this method is not suitable to use finding OD center.

Figure 4.4 A hard exudate image and OD centers. Positive sign (+) is used to show OD center which detected by ophthalmologist and star shape (*) is used to show method II.

Unlike the method I and method II, our method is able to detect OD center even in hard exudates images. In our method, ellipsoid-shaped Structuring Element (SE) provides the elimination vessels and exudates which SE does not fit into, while keeping the OD. Elimination of the exudates provides more accurate OD center coordinates than the other two methods. Another advantages of our method, it does not require the complex mathematical equations like computing the edge pixels or masking procedure and therefore computational complexity is lower than others.

Figure 4.5 A hard exudate image and OD centers. Positive sign (+) is used to show OD center which detected by ophthalmologist and cross sign (×) is used to show method III.

All three methods failed to find the correct OD center for the remaining 30 fundus images. To clear out the reason for failed performance of all methods, images' quality and demographic data of the 30 images are analyzed.

In point of images' quality, almost all 30 fundus images contain some other bright lesions which are not exudates and exudates too. As can be seen Figure 4.6, difference of the brightness among the image is effected the performance of the methods. Therefore, accuracy of methods is dependent on the experimental conditions. These lesions are more brighter than OD, therefore the methods can not catch the true center. To get scientific solutions to the problems and to increase the performance of the method III some other morphological operators should investigated. This issue forces algorithm designers to confront tradeoff between brightness of the image and accuracy of the methods which used to detect the OD center.

<p style="text-align:center;">(a)   (b)</p>
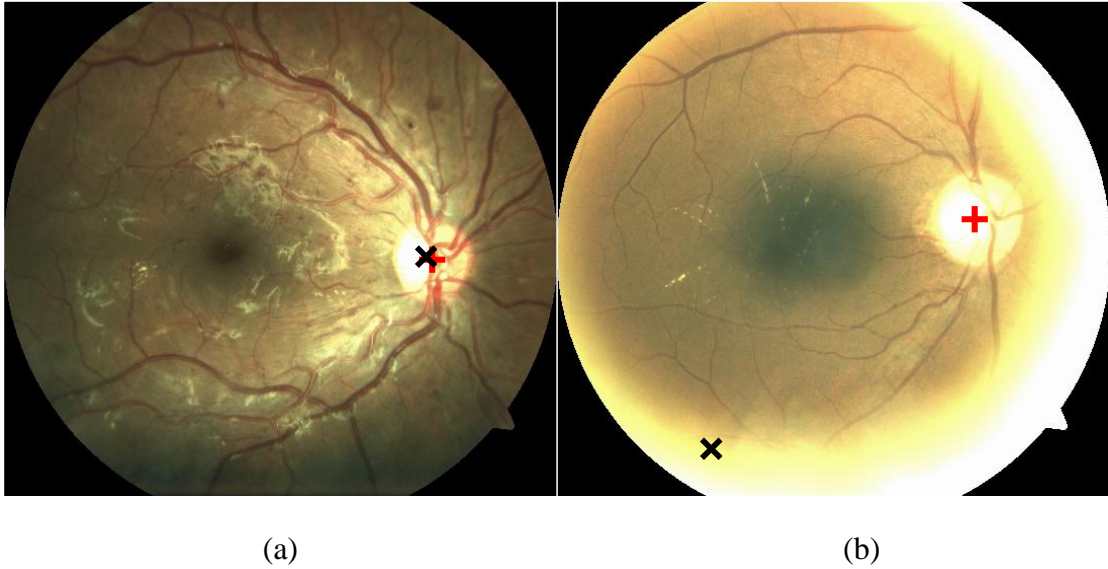
Figure 4.6 Comparison of OD center which detected by method III: A hard exudate image selected from 139 fundus images shown in (a), A hard exudate image selected from 30 fundus images shown in (b). Positive sign (+) is used to show OD center which detected by method I, and cross sign (×) is used to show method III.

In point of demographic data, the distribution of the ethnicity is analyzed (Figure 4.7). Although there is not dominant ethnic group in 30 images, the number of African is more than others. Therefore to find out the effect of African ethnicity to failed performance, a new study should set which its dataset consist of two groups as African and Caucasian.
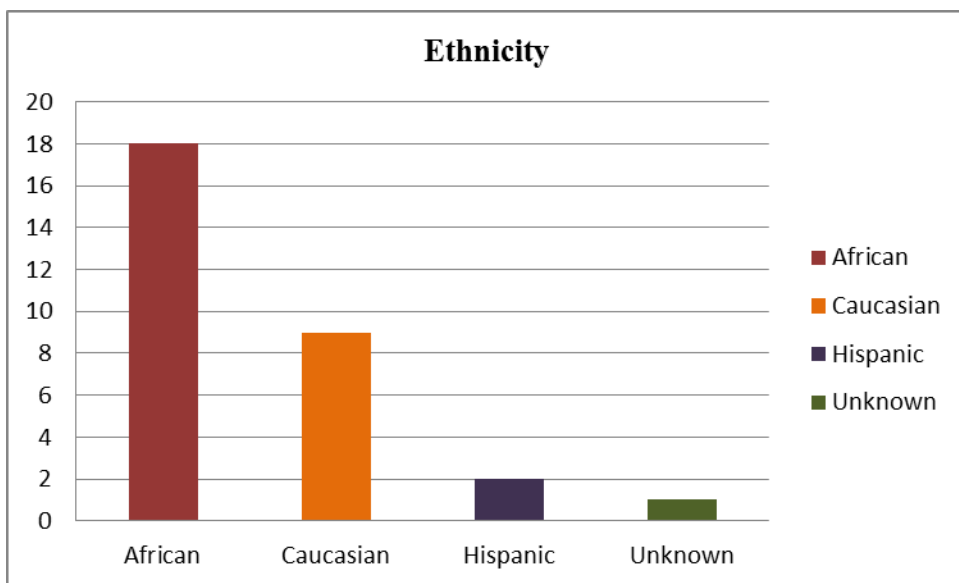
Figure 4.7 Distribution of ethnicity for the rest 30 images

CONCLUSIONS

In this thesis, we have proposed a new method for automatic detection of the optic disk based on mathematical morphological approach as Method III. All methods are tested for hard exudates and non-hard exudates images. The results indicate that the method III is more robust than method I and II in terms of computation time and finding the true coordinate for OD center especially for hard exudates fundus images.

In 139 cases method III successfully detected the location of the OD. This means that method III has potential to detect the location of the OD as %82 in fundus images with hard or non-hard exudates. An important advantage of the method III is its speed. It takes few minutes than other methods. A conference paper which has experimental results of the thesis is submitted to XIII Mediterranean Conference on Medical and Biological Engineering and Computing– MEDICON 2013

Further studies are needed to contain supplemental characteristics of the OD to improve the efficiency of detection. And finally, our proposed new method needs to be tested using other databases in terms of a more general applicability.

REFERENCES

[1]   Alghadyan, A.A.,(2011). "DR an update review". Saudi Journal of Ophthalmology, Volume 25, Issue 2, Pages 99-111.

[2]   Baker, L.M., Hand, J.P., Wang, J.J., Wong, Y.T., (2008). "Retinal signs and stroke: revisiting the link between the eye and brain". Stroke, 39(4):1371–1379, Apr 2008.

[3]   Giancardo L., Meriaudeau F., Karnowski P. T., Li Y., Garg S., Jr W. T., Kenneth, Chaum Edward. (2011) "Exudate-based diabetic macular edema detection in fundus images using publicly available datasets" Medical Image Analysis, Volume 16, Issue 1, January 2012, Pages 216-226.

[4]   Abramoff, M.D., Niemeijer, M., Suttorp-Schulten, M.S.A., Viergever, M.A., Russell, S.R., van Ginneken, B., (2008). "Evaluation of a system for automatic detection of diabetic retinopathy from color fundus photographs in a large population of patients with diabetes". Diabetes Care 31, 193–198.

[5]   Philip, S., Fleming, A.D., Goatman, K.A., Fonseca, S., McNamee, P., Scotland, G.S., Prescott, G.J., Sharp, P.F., Olson, J.A., (2007). "The efficacy of automated ''disease/no disease'' grading for diabetic retinopathy in a systematic screening programme". British Journal of Ophthalmology 91, 1512–1517.

[6]   Fleming, A.D., Goatman, K.A., Philip, S., (2010). "The role of haemorrhage and exudate detection in automated grading of diabetic retinopathy". British Journal of Ophthalmology.

[7]   Niemeijer, M., Abràmoff, M. D., & Van Ginneken, B. (2007). "Segmentation of the optic disc, macula and vascular arch in fundus photographs". Medical Imaging, IEEE Transactions on, 26(1), 116-127.

[8]   Walter, T., Klein, J. C., Massin, P., & Erginay, A. (2002). A contribution of image processing to the diagnosis of diabetic retinopathy-detection of exudates in color fundus images of the human retina. Medical Imaging, IEEE Transactions on, 21(10), 1236-1243.

[9]   Stanley E. Gunstream. Anatomy and Physiology with Integrated Study Guide (3rd ed).

[10]   Reymond, P, (2005). Digital Fundus Images Analysis: Optic Disc Centre and Boundary Detection, Fovea Localisation and Vessel Segmentation, Msc Thesis, Ecole Polytechnique f ́ed ́erale Lausanne, Switzerland

[11]   Niemeijer, M., (2006). Automatic detection of Diabetic Retinopathy in Digital Fundus Photographs, Ph.D. Thesis, Image Sciences Institute, University Medical Center Utrecht, Utrecht, The Netherlands.

[12]   LensShopper. Anatomy of the eye.

[13]   Optic disc - Wikipedia, the free encyclopedia. http://en.wikipedia.org/wiki/Optic_disc.

[14]   Wikipedia. Eye — wikipedia, the free encyclopedia, (11,05,2013)

[15]   Macula of retina - Wikipedia, the free encyclopedia. http://en.wikipedia.org/wiki/Macula.

[16]   Fovea centralis - Wikipedia, the free encyclopedia. http://en.wikipedia.org/wiki/Fovea.

[17]   U R Acharya, C M Lim, E Y K Ng, C Chee and T Tamura. Computer-based detection of diabetes retinopathy stages using digital fundus images.

[18]   C.M.R. Caridade, A.R.S. Marcal & T. Mendonca. The use of texture for image classification of black & white air-photographs.

[19]   Cassini Lossy Compression. http://www.astro.cornell.edu/research/projects/compression/entropy.html.

[20]   Rajendra Acharya U, Eddie Y. K. Ng, Jasjit S. Suri. Image Modeling of the Human Eye.

[21]   Jagadish Nayak, P Subbanna Bhat, Rajendra Acharya U, C M Lim, Manjunath Kagathi. Automated Identification of Diabetic Retinopathy Stages Using Digital Fundus Images.

[22]   Wong Li Yun, Rajendra Acharya U, Y V. Venkatesh, Caroline Chee, Lim Choo Min, E.Y.K.Ng. Identification of Different Stages Of Diabetic Retinopathy Using Retinal Optical Images.

[23]   John Paul Vetter. Biomedical Photography.

[24]   Gillian C. Vafidis. Features of diabetic eye disease.

[25]   Giancardo, L. (2011). "Automated fundus images analysis techniques to screen retinal diseases in diabetic patients", Ph.D. Thesis, Université de Bourgogne, France.

[26]   Early Treatment Diabetic Retinopathy Study Research Group: (1991) Early Treatment Diabetic Retinopathy Study design and baseline patient characteristics: ETDRS report number 7. Ophthalmology 98 (Suppl. 5):741–756.

[27]   Joussen, A., Gardner, T., and Kirchhof, B. (2007). Retinal vascular disease. Springer Verlag.

[28]   K R Bishai An inexpensive method of indirect opthalmoscopy.

[29]   Wendy Strouse Watt, O.D. Fluorescein Angiogram.

[30] CARL ZEISS Visucam PRO NM/FA Fundus Camera, http://www.dotmed.com/virtual-tradeshow/category/Ophthalmology/Fundus-Camera/Models/Carl-Zeiss/Visucam-Pro-NmFa/16421(11,05,2013)

[31] FundusPhotography. http://www.aetna.com/cpb/medical/data/500_599/0539.html.

[32] Diabetic Retinopathy Treatment - Treatment of Diabetic Retinopathy. http://vision.about.com/od/diabeticretinopathy/a/Diabetic_Retinopathy_Treatm ent.htm.

[33] Retina-Vitreous Center Procedures. http://www.retinavitreouscenter.com/procedures_laser_photocoagulation.html.

[34] Smith, W.S., (1999). The Scientist and Engineer's Guide to Digital Signal Processing, 2nd edition, California Technical Publishing, San Diego, California.

[35] Hipwell, et al., (2000) "Automated detection of microaneurysms in digital red-free photographs: a diabetic retinopathy screening tool", Diabet. Med. 17 (2000), pp. 588–594.

[36] Gonzalez, C.R., Woods, E.R., Eddins L.S., (2009). Digital Image Processing Using MATLAB, 2nd Edition, Gatesmark Publishing, Knoxville, TN.

[37] Digital ImageProcessing, http://en.wikipedia.org/wiki/Digital_image_processing

[38] Ming, F.Y., (2009). Identification of Diabetic Retinopathy Stages using Digital Fundus Images using Imaging, Final Project, School of Science and Technology, SIM University, Clementi, Singapore.

[39] Morphology Fundamentals: Dilation and Erosion: Morphological Operations (Image Processing Toolbox™). http://www.mathworks.com/help/toolbox/images/f18-12508.html.

[40] Create morphological structuring element (STREL) – MATLAB. http://www.mathworks.com/help/toolbox/images/ref/strel.html.

[41] Zhu, X., & Rangayyan, R. M. (2008, August). "Detection of the optic disc in images of the retina using the Hough transform". In Engineering in Medicine and Biology Society, 2008. EMBS 2008. 30th Annual International Conference of the IEEE (pp. 3546-3549). IEEE.

[42] Haar, F.,(2004).Automatic localization of the optic disc in digital color images of the human retina, Msc. thesis, Institute of Information and Computing Sciences, Utrecht University, Utrecht, The Netherlands.

[43] Hoover, A., Goldbaum, M., (2003). "Locating the optic nerve in a retinal image using the fuzzy convergence of the blood vessels". IEEE Transactions on Medical Imaging 22, 951–958.

[44] Niemeijer, M., Staal, J., van Ginneken, B., Loog, M., Abramoff, M.D.,(2004). "Comparative study of retinal vessel segmentation methods on a new publicly available database". Proceeding of SPIE Medical Imaging 5370, 648–657.

[45] ARIA, 2006. Retinal image archive. <http://www.eyecharity.com>.

[46]   Kauppi, T., Kalesnykiene, V., Kamarainen, J.K., L, L., Sorri, I., Uusitalo, H., Pietila, J., Kalviainen, H., Uusitalo, H., (2007). The DIARETDB1 diabetic retinopathy database and evaluation protocol. In: Proceedings of British Machine Vision Conference.

[47]   Messidor, (2010). Methods to evaluate segmentation and indexing techniques in the field of retinal ophthalmology. <http://www.messidor.crihan.fr>.

[48]   Niemeijer, M., van Ginneken, B., Cree, M.J., Mizutani, A., Quellec, G., Sanchez, C.I., Zhang, B., Hornero, R., Lamard, M., Muramatsu, C., Wu, X., Cazuguel, G., You, J., Mayo, A., Li, Q., Hatanaka, Y., Cochener, B., Roux, C., Karray, F., Garcia, M., Fujita, H., Abramoff, M.D.,(2010). "Retinopathy online challenge: automatic detection of microaneurysms in digital color fundus photographs". IEEE Transactions on Medical Imaging 29, 185–195.

[49]   Zana, F. and Klein, C.J., (2001). " Segmentation of vessel-like patterns using mathematical morphology and curvature evaluation". IEEE Trans Image Process, 10(7):1010–1019.

[50]   http://vibot.u-bourgogne.fr/luca/heimed.php

APPENDICES

APPENDIX A

Table A.1 OD center coordinates which detected by three methods from hard exudates fundus images.

Manual		Method I		Method II		Method III	
x_0	y_0	x	y	x	y	x	y
302	920	740	617	686.9	845.5	400	928
587	788	566	789	577.8	776.4	594	800
1625	737	1657	1018	1582	713.3	1596	736
1568	875	911	628	1514.9	847.8	1560	864
575	854	1339	876	583.6	845.5	585.8	848
635	935	641	952	648.7	912.3	638	988
539	884	1267	862	520	869.7	555.8	896.1
1619	971	1697	961	1586.9	936.2	1568.9	948.8
548	788	490	902.5	525.9	766.8	556	776
569	908	600	952	532.3	847	572	888
1745	806	1785	885	1708.3	774.6	1.717.5	797.5
599	779	1212	578	595.5	747.9	612	778
539	833	1559	939	493.3	836.1	543.8	842.7
1655	866	413	766	1618.4	847.2	1626.3	871.9

1643	911	1.240.5	1264	1610	879.3	1632	908
479	851	376	865	487.7	817.6	504	854
1859	686	797	584	1810.7	627.6	1832	664
1598	884	1611	1011.4	1563	845.4	1588	836
1580	857	1685.5	908.5	1551.6	846.9	1582.5	833.5
1742	845	1216.5	1193.3	1742.5	812.3	1672	828
1598	917	1451	931	1560	894.4	1603.2	914.9
1703	1022	1327	1035	1528.3	1062.8	1680.6	1011.1
1661	851	1711	726	1614.6	811.9	1644	848
554	866	569	882.3	530.8	859.9	578.5	854.5
1673	935	1771	879	1676	905.6	1647.1	909.9
476	932	471	879	1871.6	1567.7	479.8	972
1637	845	1016	930	1567.6	819.9	1620	836
1628	899	1031.5	939.5	1553.3	856.2	1611.9	934.2
335	698	290	750	320.4	667.4	348	698
488	857	430	908	454.2	834.2	486.2	852
1718	941	1464.7	1444.3	1684.8	903	1712.1	917.9
1784	842	996.3	1038.7	1744.3	812.8	1768	836
1763	935	428.5	980.5	1714.3	1025.5	1748.9	952.1
536	920	518	761	475.1	913.6	542.1	933.9
527	914	1151	717	533.7	879.6	538	892
572	905	463	867	555.9	882.9	580	888
1661	917	1603	1047	1609.6	874.9	1592.8	903
1625	989	1522	579	1470.5	971.2	1632	1018
515	800	1217.5	1326.5	492	900.9	508	826
1721	881	1790	793	1721.3	847.2	1712	880
503	947	446	809	506.5	1014	530.4	963.2

188	698	1969	1688.5	2004.6	1609.8	308	680
1589	854	1502.5	1297	1593.1	826	1577.2	837.3
533	794	1640	1116	1645.1	1108.5	557.6	825.4
533	962	498	1018.5	524.5	935.8	600.1	979.6

Table A.2 OD center coordinates which detected by three methods from non-hard exudates fundus images.

Manual		Method I		Method II		Method III	
x_0	y_0	x	y	x	y	x	y
446	869	421	918	454.7	851.7	458.2	860.1
1769	713	1727	666	1699	682.5	1748	718
1751	746	1693.5	780	1691.1	719.3	1718	742
1709	899	1732	911	1634.7	845.7	1674	908
1652	893	1658.5	736	1569.5	861.3	1608	878
467	887	514	847	442.6	860.7	484	898
461	899	573	1404	406.4	902.7	400.8	970.1
1868	659	1589	1000	1852.4	641.2	1858.2	663.9
1868	608	1270.5	657.5	1818.9	577	1826	610
1625	923	1484	834.5	1564.8	893.3	1568.1	962.2
557	914	538	796	583.2	875	561.9	860.7
1895	779	1881	750	1830.7	746.6	1806	761
227	605	243	569	224.7	575.7	288	600
1910	953	1904	898.5	1844.9	910.1	1892.5	962.2
353	884	454	953	344.4	857	330	872
1925	854	1676	1271	1917.5	821	1892.2	854

1622	905	1662	1031	1625.4	863.5	1609.5	886.5
518	854	470	758	494	833	552	852
452	977	428	987	461.1	938.1	488	996
1757	956	1637	849	1692.2	923	1720	952
1691	875	1790	834	1638.4	832.5	1668	848
1625	905	1716	875	1582.5	881.5	1612	912
329	911	330	1101.3	324.3	884	324	888
1781	1025	1606	1322	1744.4	1005.1	1764.2	1020.1
1712	956	1813	902	1666.6	938.4	1687.5	949.4
1685	935	1537	987	1642.9	883.6	1664	908
1832	746	1028	1389	1781.2	730.5	1796	772
323	749	405	702	332.8	753.8	351.6	736.1
1742	971	1360	834	1699.6	956.4	1734	976
1670	899	1572	1016	1600.9	962.3	1570	876
1772	716	1674.5	895	1736.6	687.6	1768	724
494	782	381	868	501.7	803.6	502	782
1808	761	1685	772	1734.1	743.9	1740	752
1697	1022	1259	1359	1642.5	999.7	1646	1020
623	947	663	1113	618	946.1	630.5	950.5
1766	986	1596	1008	1697.7	948.6	1740	968
509	893	795	883	521.4	892.4	541.4	893.4
1775	875	1840	982	1715.5	850.6	1749.5	873.5
1682	962	1674	764	1616.6	939.2	1655.9	963.8
1712	905	1969	1688.5	1646.6	884.9	1690	904
326	599	457	602	346	582.9	348	592
1907	659	1908	702.5	1857.6	635	1872	664
1850	929	1879	953	578.8	62.6	1817.5	926.5

1721	923	1723	985	1676.2	896.5	1704	918
1880	665	882	971	1824.7	647.1	1851.5	667.4
602	899	661	879	596.1	872.6	617.5	909.5
1640	755	1630	704	1613.9	744	1648	740
1580	920	1523	872	1514.1	894.5	1552	928
1649	920	1554	906	1612.7	900.7	1656	912
2120	926	1987	1661	144.5	1452.3	2056	934
1649	830	1643	1095	1646.3	798.1	1625.8	834
1688	896	1713	844	1632.1	891.6	1628	923.8
1640	899	1610	1236	1600.9	879.2	1597.3	879.4
1598	908	1098.5	1928	1537.3	850.8	1528.8	885.3
2105	965	1982	908	2023.3	957.9	2049.3	978.6
1730	854	1833	905	1685.2	830.3	1710	846
497	908	1969	1688.5	563.6	891.8	607.1	926.8
1619	896	1637	890	1539	868.1	1516.2	932.5
1694	887	1783	826	1552	788.3	1680	880
1607	947	1680	1059	1556.1	940.4	1578	958
1727	983	1261	1271	1679.3	941.8	1708	968
1685	998	1553.5	737.5	1612	975.4	1676	996
1715	929	1700.5	1118.8	1721.2	914	1692	920
1583	941	1546.5	996.5	1515	917.6	1520	936
1646	815	987	1414	1619.8	790.9	1648	806
1730	995	1457	462	1748.9	998.3	1737.2	997.3
1679	962	1432.5	1156	1679.1	942	1666	960
1619	953	1651	942.3	1555.6	900.2	1602.2	938
1640	941	1621	820	1586.8	894.1	1630	926
1886	1058	1576.8	972.7	1808.2	1032.3	1862	1056

1736	956	1515	1235	1647.2	975.9	1740.8	987.2
1571	776	1535	1035	1543.3	792.8	1560.4	787.9
1901	659	1853.3	649.7	1852.9	632.3	1863.6	680.5
1652	863	1743	798	1591.6	842.8	1608	868
1661	995	1435	402	1563	831.1	1623.9	950
1640	893	1712	952	1628.7	874.9	1636	872
1640	899	1700	871	1612.4	864.6	1626	898
1685	920	1725	1077	1682.3	889	1696	918
1691	905	1659.7	935.7	2086.9	1228.3	1656.9	933.9
1685	905	1691	878.5	1602.7	857	1575.9	916.6
1739	893	1730	701	1733.8	877	1711.7	875.4
1670	989	1554	984	300.8	1670.9	1664	988
638	845	506	868	633.9	836.1	644	840
1586	971	1650	872	1533.5	930.9	1568	956.9
1640	929	1623	1180	1657.6	876.8	1636.8	883.8
1601	935	1673	949	1551.5	911.9	1507.3	882.5
1709	911	1653	889	1618.2	924.9	1638.1	829.6
578	857	619	968	592.2	817.5	598.2	852
1592	953	1586.7	934.3	1551.3	922.1	1520	948
512	911	688	961	549.3	903.9	604	928
1634	854	1642.5	864	1569.4	857.7	1560.7	874.9
1826	752	1809	737	1710.7	721.5	1760	764
614	932	661	955	236.5	1665	652	940
1634	959	1534	1046	1603.6	943.9	1620	950

Table A.3 All the methods detected OD center coordinates wrongly from the rest of 30 fundus images.

Manual		Method I		Method II		Method III	
x_0	y_0	x	y	x	y	x	y
1709	839	1489	395	1614.9	848.1	1499.7	1173.2
1571	869	1516	937	1477.9	832	1133.6	541.4
1721	884	1744	735	1656.9	894.5	1688	508
524	881	469	708	530.7	856.2	308	1244
1652	875	1654	1077.5	1568.3	844	704	1904
1739	965	1786	907	1569.1	806.2	1434.4	488.3
590	884	548	713.5	1983.3	1446.4	2142	984
1676	827	1363.3	1576.8	1578.9	981.8	718	1214
1661	863	1987	1661	1541.6	1153.8	616	1772
509	848	428	893	481.2	814.4	928.9	426.1
554	887	1204	1032	550.3	888.8	892	1252
539	875	525	785	487.9	844.3	1630	1774
524	851	504	683	522.1	849.8	748	1266
1655	905	1568	499	1539.8	821.2	1666	1292
1682	881	824	779	580.8	617.3	642.6	638.6
1889	692	1892	682	1766.4	751.6	1581.1	1033.8
1658	920	1584	689	1546.8	772.7	1296.1	575.2
1667	842	1431	1253	1619.5	820.6	1500	1132
566	866	454	865	565.4	769.7	822.1	1227.2
1784	734	1881	744	1705.6	868.8	1925.3	508.8
1646	887	1703	1055	1634.4	961.4	1372	1152
1646	908	1367	294	1621.6	856.2	1223.2	1264.6
1571	959	1596	1081	1503.3	937.8	333.5	953.5

1694	854	1663	484	1604.1	849.7	599.1	998.5
1583	848	1678	791	1521.4	827.6	1407.2	1219.3
1637	1004	1639	951	1639	977.7	1404.7	717.4
434	836	408	729	379	828.5	508	1332
1625	875	1644	894	1536.7	929.7	1642	1380
1646	899	1732	984	1593	882.7	1667.4	1461.7
1664	887	1699	996	1562.8	852	1342.5	673.5

CURRICULUM VITAE

Name Surname: Raziye Yağız

Place and Date of Birth: Denizli/21.04.1989

Address: Cahitzarifoğlu cad.Başakşehir mah.Onurkent sitesi
No:14B/13 Başakşehir/İstanbul

E-Mail: raziyeyagiz@gmail.com

B.Sc.: Fatih University, Mathematics,3.88/4.0, First Ranked
Graduate in Department, İstanbul, 2007-2011.

Scholarship: 2012 Scholarship for summer internship, provided by
ERASMUS

2011-2013 Scholarship for M.S. Degree, Provided by

TÜBİTAK (The Scientific &Technological Research

Council of Turkey).

Experience: 2012, Summer ERASMUS internship, Lübeck University,

Institute for Signal Processing, Software Engineering,

Germany.

Research interest: Biomedical Image Processing, Biomedical Signal

Processing.